Studies on Highly Luminescent Mononuclear Copper(I)-Halide Complexes with N-heteroaromatic ligands

(N-ヘテロ芳香族配位子を有する強発光性ハロゲン化銅(I) 単核錯体に関する研究)

Graduate School of Chemical Sciences and Engineering, Hokkaido University

Hiroki Ohara

Contents

Chapter 1

General Introduction

1-1 Luminescent Metal Complexes

Luminescent materials, which are used for illumination and display devices, are required for our lives. Various luminescent compounds have been developed to improve the luminescence efficiency, durability, convenience and so on. Especially, luminescent transition metal complexes have played a leading role in the development of such devices because these complexes exhibit diverse emissive excited states involved in metal ion and organic ligands. Luminescent transition metal complexes also have attracted much attention because of their potential application for solar energy conversion, luminescence based sensors, organic light-emitting diodes (OLEDs) and probe of biological systems.

In particular, phosphorescent materials based on precious-metal complexes such as Ir(III) and Pt(II) have been developed increasingly as useful emitters for efficient light generation in OLEDs.[1] These precious-metal complexes exhibit phosphorescence from triplet metal-to-ligand charge-transfer (MLCT) states and ligand-based excited states due to strong spin-orbit coupling. The emission from MLCT and/or ligand-based excited states enables an efficient tuning of the emission color by varying the ligands. For example, Bernhard and co-worker reported bis-cyclometallated Ir(III) complexes $[Ir(C^N)_2(N^N)]PF_6$ (C^N = cyclometalating ligands, N^N = diimine ligands) which exhibit various emission color by changing the C^N and N^N ligands (Figure 1-1).[2]

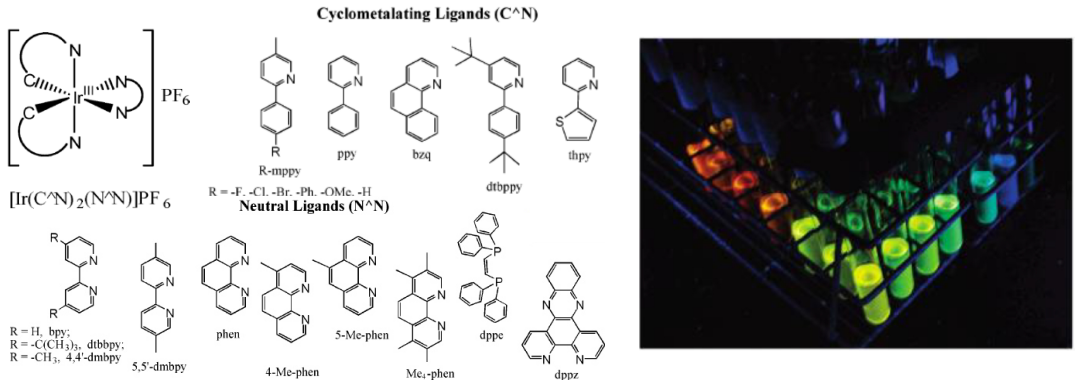

Figure 1-1.Molecular structure (left) and emission image (right) of $[Ir(C^N)_2(N^N)]PF_6$ complexes.[2]

In another instance, cyclometalated tetradentate Pt(II) complexes [Pt(N^C-O-LL')] (N^C = cyclometalating ligand moiety, LL' = ancillary ligand moiety such as phenoxy-pyridine, Scheme 1-1, **1**-**3**) show blue to green emission with high quantum yield of 0.39 to 0.64 in solution.[3] When doped in a poly(methylmethacrylate) (PMMA) thin film, measured quantum efficiencies increase to 0.81–0.97.

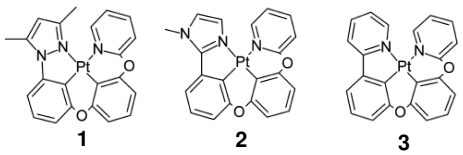

Scheme 1-1.Molecular structure of Pt complexes **1**-**3**.

Luminescent d^{10} metal complexes such as Au(I) and Cu(I) also have been extensively studied because of their interesting photoluminescence properties. In d^{10} metal complexes, the d-d excited state which provide cause of the non-radiative decay process is not generated, thus these complexes can be promising luminescent materials for application. Ito et al. reported mechanochromic luminescence of phenyl(phenyl isocyanide)gold(I) (**4**, Figure 1-2).[4] A kinetically isolated polymorph of this compound is caused single-crystal-to-single-crystal transformation to thermodynamically stable polymorph by small mechanical stimulus or solid seeding and the luminescent color varies blue to yellow associated with single-crystal-to-single-crystal transformation.

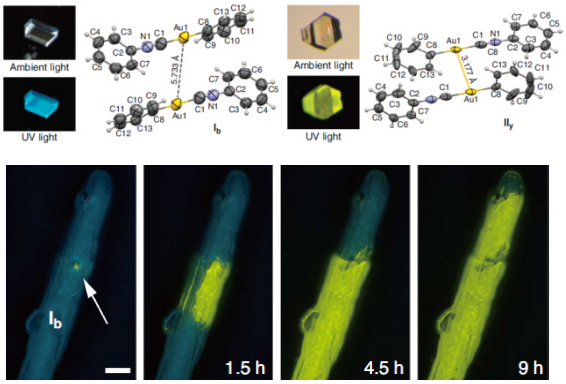

Figure 1-2. Photos under ambient and ultraviolet light and crystal structure of two polymorph of **4** (upper). Mechanical stimulus-triggerd phase transformation of **4** crystal (bottom).[4]

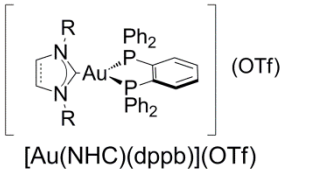

[Au(NHC)(dppb)](OTf)

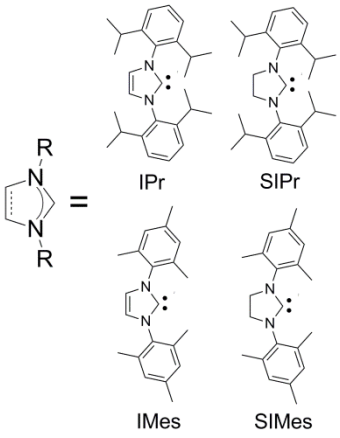

Scheme 1-2. Molecular structure of [Au(NHC)(dppb)](OTf).

Recently, highly luminescent three-coordinate Au(I) N-heterocyclic carbene complexes [Au(NHC)(dppb)](OTf) (NHC = N-heterocyclic carbine, dppb = 1,2-bis(diphenylphosphino)benzene, Scheme 1-2) were reported.[5] These complexes exhibit high luminescence quantum yields of ~0.99 in the solid state and the emissive states are assigned to ligand (dppb) to metal-ligand (Au-NHC) charge-transfer (LML'CT) states.

Various types of luminescent Cu(I) complexes also have been reported and we discuss these complexes in the next section.

1-2 Luminescent Cu(I) Complexes

Although various types of luminescent metal complexes have been reported so far, most of luminescent complexes with efficient emission are noble metal complexes as noted above. Consequently, low-cost alternative materials came into the focus of research as those of the next-generation. Among Luminescent d^{10} metal complexes, Cu(I) complexes have received increased attention because these complexes are inexpensive, abundant and exhibit intense photoluminescence properties. $[Cu(dmp)_2]^+$ (dmp = 2,9-dimethyl-1,10-phenanthroline) is well known for research on luminescent Cu(I) complexes and the photoluminescence properties of this complex were investigated.[6] The lowest excited state of $[Cu(dmp)_2]^+$ is assigned to MLCT state, thus the excited state closely resemble the Cu(II) state which has d^9 electronic configuration. The oxidation in the excited state cause structural distortion from the tetrahedral to the flattened structure and this structural distortion accelerate the non-radiative decay process (Figure 1-3). The structural distortion to flattened structure also allow to solvent attack and exciplex formation which caused non-radiative decay process. The complexes of 1,10-phenanthroline ligands with bulkier substituents such as *sec*-butyl (dsbp) and neopentyl (dnpp) groups at the 2,9-positions exhibit higher luminescence quantum yields in CH_2Cl_2 compared to that of $[Cu(dmp)_2]^+$ (Scheme 1-3).[7] The introduction of the bulky substituents at the 2,9-positons of the phenanthroline ligand effectively suppresses the structural distortion in the excited state and lead to the high luminescence quantum yields. Therefore, inhibition of the structural distortion in excited state play a significant role in the attainment of efficient emission. However, these bisdiimine Cu(I) complexes exhibit low luminescence quantum yields (< 0.01) in solution.

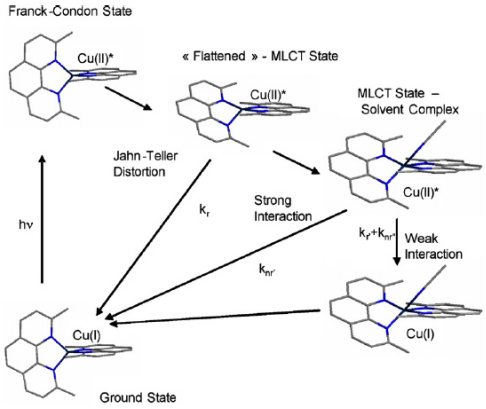

Figure 1-3. Representation of dynamic excited-state processes in $[Cu(dmp)_2]^+$ complex including interaction with acetonitrile solvent molecule.[6d]

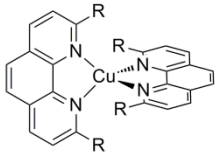

R = Methyl Φ = 0.0004
R = *sec*-Butyl Φ = 0.0045
R = Neopentyl Φ = 0.0016

Scheme 1-3. Molecular structure and luminescence quantum yield in CH_2Cl_2 of $[Cu(dmp)_2]^+$, $[Cu(dsbp)_2]^+$ and $[Cu(dnpp)_2]^+$.

To achieve efficient luminescence of Cu(I) complexes, mononuclear diimine/diphosphine mixed-ligand Cu(I) complexes $[Cu(NN)(PP)]^+$ (NN = diimine ligands, PP = diphosphine ligands) have been synthesized and investigated their photoluminescence properties. McMillin and Walton reported that $[Cu(dbp)(POP)]^+$ (dbp = 2,9-di-*n*-butyl-1,10-phenanthroline, POP = bis[2-(diphenylphosphino)phenyl]ether) exhibited

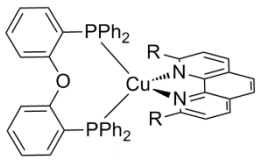

R = *n*-Butyl Φ = 0.16

Scheme 1-4. Molecular structure and luminescence quantum yield in CH_2Cl_2 of $[Cu(dbp)(POP)]^+$.

high quantum yield of 0.16 in dichloromethane solution (Scheme 1-4).[8] Armaroli and Nierengarten also reported $[Cu(dmdpp)(POP)]^+$ (dmdpp = 2,9-dimethyl-4,7-diphenylphenanthroline) with the high quantum yield of 0.28 in dichloromethane solution (Scheme 1-5).[9] The bulky diphosphine ligand such as POP suppresses the flattening distortion more effectively compared to diimine ligands, leading to high luminescence quantum yields in solution.

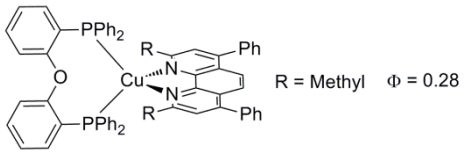

Scheme 1-5. Molecular structure and luminescence quantum yield in CH_2Cl_2 of $[Cu(dmdpp)(POP)]^+$.

Halide-bridged multinuclear Cu(I) complexes also have been studied their photoluminescence properties in detail. Especially, tetranuclear cubane-type complexes with pyridine or phosphine ligands (L) $[Cu_4(\mu_3\text{-}X)_4L_4]$ have been extensively investigated and many compounds with their luminescent properties have been reported.[10] $[Cu_4(\mu_3\text{-}I)_4(py)_4]$ (py = pyridine) exhibit strong emission and luminescent maxima of this complex is 580 nm in solid state at 294K (Figure 1-4).[11] The nature of the emission properties is due to an electron migration from a non-bonding orbital constructed by metal d electrons or halogen p electrons to an empty bonding in-phase orbital contributed from the s/p atomic orbitals in the center of the complex. Density functional theory (DFT) calculation demonstrated that emission can be attributed to the triplet cluster centered (^{3}CC) excited state in which an electron is located on a bonding in-phase orbital constructed from s/p atomic orbitals of the four metal atoms. On the other hand, the emission maxima shift toward longer wavelength (λ_{max} = 619 nm) and new emission peak appear at shorter wavelength side at 77K (λ_{max} = 438 nm). The additional emission peak appearing at low temperature is assigned to a halogen-to-ligand charge transfer (XLCT) state. This spectral change with temperature alteration is referred to as "luminescence thermochromism" or "thermochromic luminescence" and originates from the temperature-dependent metalophilic (Cu···Cu) interaction in the tetranuclear cluster core.

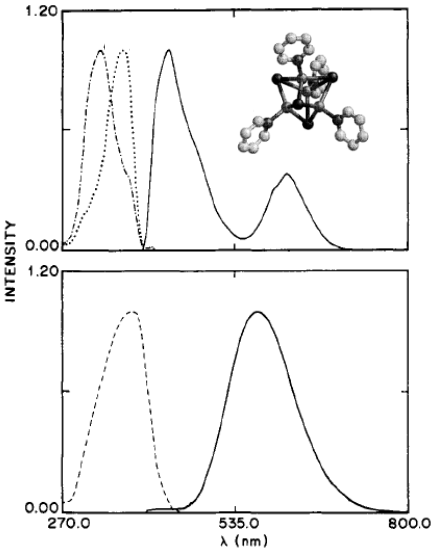

Figure 1-4. Excitation and emission spectra of $[Cu_4(\mu_3\text{-}I)_4(py)_4]$ at 77K (upper) and 294K(lower); inset: molecular structure of $[Cu_4(\mu_3\text{-}I)_4(py)_4]$.[11]

Boilot et al. reported mechanochromic luminescence of tetranuclear Cu(I)-iodide complex $[Cu_4(\mu_3\text{-}I_4)(PPh_2(CH_2CH{=}CH_2))_4]$ (Figure 1-5 (a)).[12] This complex exhibit green emission (λ_{max} = 530 nm) in powder under UV irradiation. After grinding using pestle, the green emission is converted into a yellow one (λ_{max} = 580 nm) (Figure 1-5(b-d)). The initial green emission is recovered by exposure to solvent or heating. The emission studies, X-ray diffraction and NMR analysis of the cluster before and after the grinding process suggests that the crystal packing where

the intermolecular arrangement is modified, thus affecting the Cu···Cu distances of the $[Cu_4(\mu_3\text{-}I_4)]$ core.

Cu(I)-halide dinuclear complexes bearing N-heteroaromatic ligands (L) can provide systematic emitters with different emission colors from red to blue. For example, $[(Cu_2(\mu\text{-}X)_2(PPh_3)_2(L)_2]$ shows strong emission and the color varies from red to blue by the systematic change of L (Figure 1-6).[13] Recently, Bräse et al. reported photoluminescence properties of dinuclear copper(I)-halide complexes with P^N Ligands $[Cu_2(\mu\text{-}X)_2(P\text{^}N)_3]$ (P^N = N-heteroaromatic compounds with a diphenylphosphino group) (Figure 1-7).[14] These complexes exhibit emission covering the visible spectrum from blue to red with high quantum yields up to 0.96. The emission wavelengths of the complexes are tunable systematically by modification of N-heteroaromatic moiety of P^N ligands. DFT calculation suggest that Cu(I)-halide dinuclear complexes emit from MLCT state mixed with XLCT state ((M+X)LCT), thus replacement of N-heteroaromatic moiety allows for systematic tuning of the luminescence color.

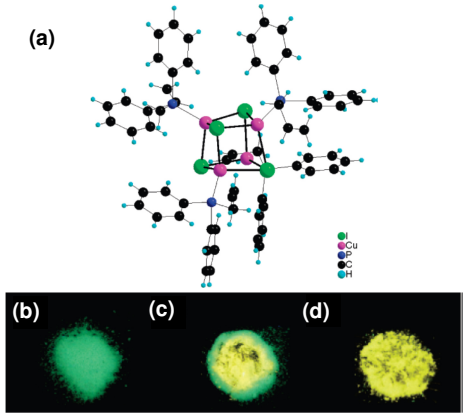

Figure 1-5. Molecular structure (a) and grinding luminescence change (b-d) of $[Cu_4(\mu_3\text{-}I_4)(PPh_2(CH_2CH{=}CH_2))_4]$.[12]

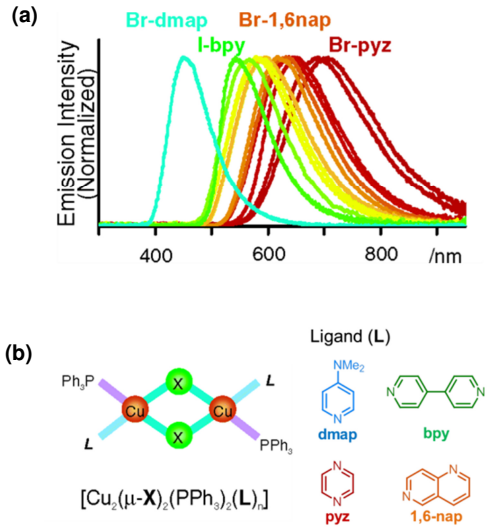

Figure 1-6. Luminescent spectra (a) and molecular structure (b) of $[(Cu_2(\mu\text{-}X)_2(PPh_3)_2(L)_2]$.[13]

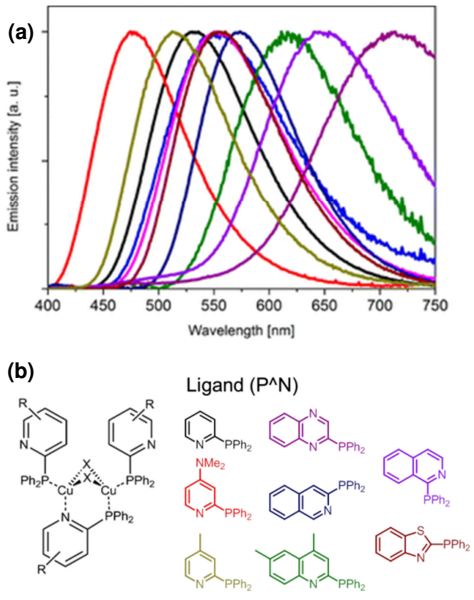

Figure 1-7. Luminescent spectra (a) and molecular structure (b) of $[Cu_2(\mu\text{-}X)_2(P\text{^}N)_3]$.[14]

1-3 Thermally Activated Delayed Fluorescence (TADF)

Phosphorescent materials based on noble metal complexes have been increasingly developed for efficient light generation in OLEDs. Phosphorescent materials are advantageous over fluorescent materials because of their ability to harvest both singlet and triplet excitons, resulting in theoretically 100% internal quantum efficiency.[15] However, these phosphorescent materials are expensive and highly limited resources. Therefore, alternative materials are being developed. Recently, thermally activated delayed fluorescence (TADF) materials based on non-noble metal complexes and organic compounds have attracted much attention because they can harvest both singlet and triplet excitons.[16] When the energy difference (ΔE) between the lowest excited singlet state (S_1) and the lowest excited triplet state (T_1) is small, the singlet state can be thermally activated at the expense of the triplet state. Adachi et al. reported highly efficient TADF emitters based on carbazolyl dicyanobenzene (CDCB) derivatives (Figure 1-8).[16a] These CDCB derivatives exhibit various emission colors from orange to blue with high photoluminescence quantum yields up 0.94 in toluene solution. The ΔE of 4CzIPN is 83 meV, indicating that the emission at room temperature is principally delayed fluorescence. Using these derivatives, very high external electroluminescence quantum efficiency of 19.3% is achieved for the green OLED.

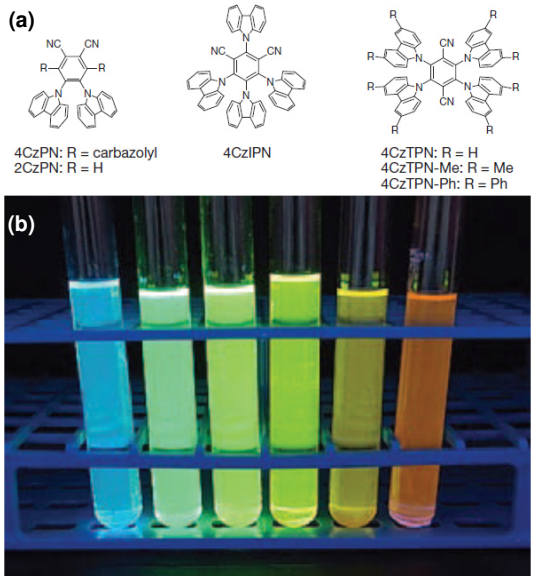

Figure 1-8. Molecular structure (a) and emission image (b) of CDCB derivatives.[16a]

Cu(I) complexes with tetrahedral geometry have great potential for the synthesis of efficient TADF materials because of the small ΔE based on the metal-to-ligand charge transfer (MLCT) state, where the stability of the triplet state is small (<ca. 1000 cm^{-1}) owing to small exchange interactions. For example, Yersin et al. reported blue-light TADF emitters of Cu(I) complexes [Cu(POP)(NN)] (NN = bidentate pyrazolylborate) (Figure 1-9).[17] These complexes exhibit high luminescence quantum yield of ~0.90 in powder and the emissive state is assigned to MLCT state involving Cu-3d and POP-π* orbitals. Investigation of spectroscopic properties and the emission decay behavior in the temperature range between 1.6K and ambient temperature revealed that the bright blue light emission at room temperature originates from delayed fluorescence caused by the

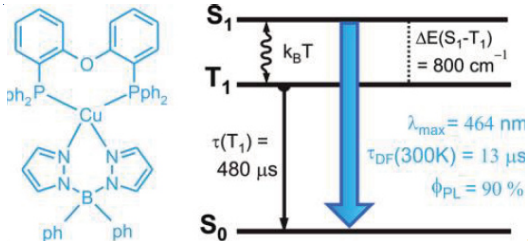

Figure 1-9. Molecular structure (left) and luminescence properties (right) of [Cu(POP)(NN)].[17]

^{1}MLCT state, which is generated by thermal activation from the ^{3}MLCT transition state because of small singlet–triplet energy differences (ΔE = 800–1300 cm^{-1}). In another instance, Deaton and Peters reported that a highly emissive dinuclear copper(I) complex $[Cu(PNP)]_2$ (PNP = bis(phosphine)diarylamido ligand) with luminescence quantum yield of 0.57 in 2-methyltetrahydrofuran was shown to exhibit TADF by variable temperature emission spectroscopy and luminescence decay measurement of doped vapor-deposited films.[16b] The lowest energy singlet and triplet states were assigned as CT states on the basis of TD-DFT calculation and small observed ΔE (786 cm^{-1}) determined by emission decay analyses. Vapor-deposited OLEDs doped with the complex in the emissive layer gave a maximum external quantum efficiency of 16.1%. Therefore, luminescent Cu(I) complexes potentially applied to OLED devices.

1-4 Mechanochemical Syntheses

Mechanochemical syntheses are reactions conducted by grinding solid reactants together with no or minimal solvent and noted for their convenience, higher yield and frequent decrease in reaction time relative to the analogous solution reaction. Mechanochemical syntheses have been used in many instances to synthesize various compounds such as metal complexes and organic compounds.[18] For example, Balema and Pecharsky reported solvent-free mechanochemical synthesis of *cis*-$(Ph_3P)_2PtCl_2$ and *cis*-$(Ph_3P)_2PtCO_3$ (Scheme 1-6).[19] These complexes are prepared by ball-milling of solid reactants in the absence of a solvent. *cis*-$(Ph_3P)_2PtCl_2$ are obtained in 98% yield after ball-milling of polycrystalline $PtCl_2$ and PPh_3 for 2 h. *cis*-$(Ph_3P)_2PtCO_3$ are also synthesized in 70% yield by ball mill grinding of *cis*-$(Ph_3P)_2PtCl_2$ with an excess of anhydrous K_2CO_3 for 14 h. The formation of these complexes as a consequence of the solvent-free mechanochemical reactions has been confirmed by means of solid-state ^{31}P MAS NMR spectroscopy, powder X-ray diffraction (PXRD) and differential thermal analysis.

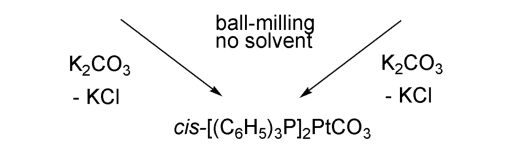

Scheme 1-6. Solvent-free mechanochemical synthesis of two Pt complexes *cis*-$(Ph_3P)_2PtCl_2$ and *cis*-$(Ph_3P)_2PtCO_3$.[19]

Recently, several luminescent Cu(I) coordination polymers were synthesized by mechanochemical approach. Lewinsiki et al. reported synthesis of luminescent Cu(I)-iodide coordination polymer $\{[Cu_4(\mu_3\text{-}I)_4(QN)_2][Cu_3(\mu_3\text{-}I)_2(\mu_2\text{-}I)(QN)_2]_2\}_n$ (QN = quinine) by solvothermal and mechanochemical synthesis (Scheme 1-7).[20] This coordination polymer is synthesized by solvothermal synthesis for 20 h and exhibit yellow emission which is attributed to halide-to-metal charge transfer (XMCT) and ^{3}CC state with localized on the Cu_3I_3 core. This coordination polymer is also prepared by ball-mill grinding and the reaction time is shorter (30 min) compared to solvothermal synthesis. Therefore, mechanochemical syntheses are a powerful technique for preparation of luminescent Cu(I) complexes.

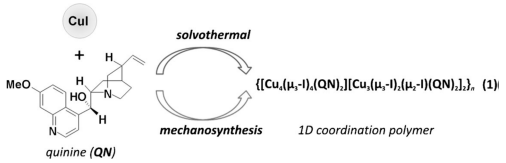

Scheme 1-7. Solvothermal and mechanochemical synthesis of $\{[Cu_4(\mu_3\text{-}I)_4(QN)_2][Cu_3(\mu_3\text{-}I)_2(\mu_2\text{-}I)(QN)_2]_2\}_n$.[20]

1-5 Purpose of this thesis

A number of studies of luminescent Cu(I) complexes have been reported until now. Although various types of luminescent Cu(I) complexes have been synthesized and investigated so far, luminescent properties of mononuclear Cu(I)-halide complexes have been reported in only a few cases. Mononuclear Cu(I) complexes are expected to be easily prepared and tunable emission properties because these complexes have simpler structure compared to other luminescent Cu(I) complexes.

In this thesis, luminescent properties of mononuclear Cu(I)-halide complexes with N-heteroaromatic ligands (L) $[CuX(PPh_3)_2(L)]$ (X = Cl^-, Br^-, I^-, Scheme 1-8) were discussed. Firstly, to demonstrate simple synthesis of luminescent Cu(I) complexes, mechanical synthesis of luminescent mononuclear Cu(I)-iodide complexes were investigated. In addition, luminescent mononuclear Cu(I)-halide complexes with various type of L were synthesized to investigate influence on luminescence properties by systematic change of L.

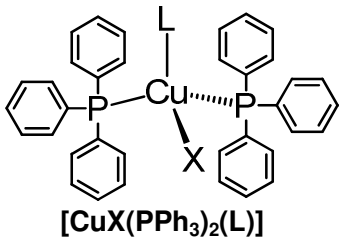

$[CuX(PPh_3)_2(L)]$

Scheme 1-8. Molecular structure of mononuclear Cu(I)-halide complexes $[CuX(PPh_3)_2(L)]$ (X = Cl^-, Br^-, I^-).

1-6 Outlines of this thesis

This thesis consists of 5 chapters as briefly described below.

In chapter 1, the research background and purpose of the thesis are described. As key aspects into the present study, the essence of luminescent metal complexes, especially Cu(I) complexes, TADF materials and mechanochemical syntheses are overviewed.

In chapter 2, the grinding synthesis and luminescence properties of three mononuclear Cu(I)-iodide complexes, $[CuI(PPh_3)_2(L)]$ (L = isoquinoline (iq), 1,6-naphthyridine (nap) and pyridine (py)) are described. These complexes were synthesized by simple manual grinding with higher yields compared to analogue solution syntheses and exhibit strong emission with high quantum yields of 0.63-0.99.

In chapter 3, simple and extremely efficient blue emitters based on mononuclear Cu(I)-halide complexes with delayed fluorescence, $[CuX(PPh_3)_2(Mepy)]$ (X = Cl^-, Br^-, I^-, Mepy = 4-methylpyridine) are described. They exhibit blue light emission with extremely high photoluminescence quantum yields, approaching 100% in the solid states. The emission lifetime analyses and DFT calculations reveal that the bright blue light emission at room temperature originates from delayed fluorescence caused by the ^{1}(M+X)LCT, which is generated by thermal activation from the ^{3}(M+X)LCT state.

In chapter 4, luminescent Cu(I) complexes bearing N-heteroaromatic ligands whose emission color depend on type of N-heteroaromatic ligands, $[CuX(PPh_3)_2(L)]$ (X = Cl^-, Br^-, I^-, L = Mepy, iq and nap) are described. These complexes show strong emission and the color varies from red to blue by the systematic change of L and halide anion.

In chapter 5, general conclusion and future perspectives of the study are summarized.

1-7 References

1 (a) L. Xiao, Z. Chen, B. Qu, J. Luo, S. Kong, Q. Gong and J. Kido, *Adv. Mater.*, 2011, **23**, 926; (b) Y. Chi and P. T. Chou, *Chem. Soc. Rev.*, 2010, **39**, 638.

2 M. S. Lowry, W. R. Hudson, R. A. Pascal, Jr. and S. Bernhard, *J. Am. Chem. Soc.*, 2004, **126**, 14129.

3 E. Turner, N. Bakken and J. Li, *Inorg. Chem.*, 2013, **52**, 7344

4 H. Ito, M. Muromoto, S. Kurenuma, S. Ishizaka, N. Kitamura, H. Sato and T. Seki, *Nat. Commun.*, 2013, **4**, 2009.

5 R. Visbal, J. M. Lopez-de-Luzuriaga, A. Laguna and M. C. Gimeno, *Dalton Trans.*, 2014, **43**, 328.

6 (a) D. R. McMillin and K. M. McNett, *Chem. Rev.*, 1998, **98**, 1201; (b) J. R. Kirchhoff, R. E. Gamache, M. W. Blaskie, A. A. Del Paggio, R. K. Lengel and D. R. McMillin, *Inorg. Chem.*, 1983, **22**, 2380; (c) M. Ruthkosky, C. A. Kelly, F. N. Castellano and G. J. Meyer, *Coord. Chem. Rev.*, 1998, **171**, 309; (d) A. Laviecambot, M. Cantuel, Y. Leydet, G. Jonusauskas, D. Bassani and N. McClenaghan, *Coord. Chem. Rev.*, 2008, **252**, 2572; (e) Z. A. Siddique, Y. Yamamoto, T. Ohno and K. Nozaki, *Inorg. Chem.*, 2003, **42**, 6366; (f) C. Kutal, *Coord. Chem. Rev.*, 1990, **99**, 213.

7 M. K. Eggleston, D. R. McMillin, K. S. Koenig and A. J. Pallenberg, *Inorg. Chem.*, 1997, **36**, 172.

8 D. G. Cuttell, S.-M. Kuang, P. E. Fanwick, D. R. McMillin and R. A. Walton, *J. Am. Chem. Soc.*, 2002, **124**, 6.

9 N. Armaroli, G. Accorsi, M. Holler, O. Moudam, J. F. Nierengarten, Z. Zhou, R. T. Wegh and R. Welter, *Adv. Mater.*, 2006, **18**, 1313.

10 (a) P. C. Ford, E. Cariati and J. Bourassa, *Chem. Rev.*, 1999, **99**, 3625; (b) H. Kitagawa, Y. Ozawa and K. Toriumi, *Chem Commun.*, 2010, **46**, 6302.

11 K. R. Kyle, C. K. Ryu, P. C. Ford and J. A. DiBenedetto, *J. Am. Chem. Soc.*, 1991, **113**, 2954.

12 S. Perruchas, X. F. Le Goff, S. Maron, I. Maurin, F. Guillen, A. Garcia, T. Gacoin and J. P. Boilot, *J. Am. Chem. Soc.*, 2010, **132**, 10967.

13 H. Araki, K. Tsuge, Y. Sasaki, S. Ishizaka and N. Kitamura, *Inorg. Chem.*, 2005, **44**, 9667.

14 (a) D. M. Zink, M. Bachle, T. Baumann, M. Nieger, M. Kuhn, C. Wang, W. Klopper, U. Monkowius, T. Hofbeck, H. Yersin and S. Bräse, *Inorg. Chem.*, 2013, **52**, 2292; (b) D. M. Zink, T. Baumann, J. Friedrichs, M. Nieger and S. Brase, *Inorg. Chem.*, 2013, **52**, 13509.

15 (a) C. Adachi, M. A. Baldo, M. E. Thompson and S. R. Forrest, *J. Appl. Phys.*, 2001, **90**, 5048; (b) H. Sasabe, J. Takamatsu, T. Motoyama, S. Watanabe, G. Wagenblast, N. Langer, O. Molt, E. Fuchs, C. Lennartz and J. Kido, *Adv. Mater.*, 2010, **22**, 5003; (c) S. R. Forrest, M. A.

Baldo, D. F. O'Brien, Y. You, A. Shoustikov, S. Sibley and M. E. Thompson, *Nature*, 1998, **395**, 151; (d) M. A. Baldo, S. Lamansky, P. E. Burrows, M. E. Thompson and S. R. Forrest, *Appl. Phys. Lett.*, 1999, **75**, 4; (e) Y. Kawamura, K. Goushi, J. Brooks, J. J. Brown, H. Sasabe and C. Adachi, *Appl. Phys. Lett.*, 2005, **86**, 071104.

16 (a) H. Uoyama, K. Goushi, K. Shizu, H. Nomura and C. Adachi, *Nature*, 2012, **492**, 234; (b) J. C. Deaton, S. C. Switalski, D. Y. Kondakov, R. H. Young, T. D. Pawlik, D. J. Giesen, S. B. Harkins, A. J. Miller, S. F. Mickenberg and J. C. Peters, *J. Am. Chem. Soc.*, 2010, **132**, 9499; (c) A. Tsuboyama, K. Kuge, M. Furugori, S. Okada, M. Hoshino and K. Ueno, *Inorg. Chem.*, 2007, **46**, 1992.

17 R. Czerwieniec, J. Yu and H. Yersin, *Inorg. Chem.*, 2011, **50**, 8293.

18 (a) A. L. Garay, A. Pichon and S. L. James, *Chem. Soc. Rev.*, 2007, **36**, 846; (b) G. A. Bowmaker, *Chem Commun.*, 2013, **49**, 334; (c) G. W. Wang, *Chem. Soc. Rev.*, 2013, **42**, 7668.

19 V. P. Balema, J. W. Wiench, M. Pruski and V. K. Pecharsky, *Chem. Commun.*, 2002, 1606.

20 D. Prochowicz, I. Justyniak, A. Kornowicz, T. Kaczorowski, Z. Kaszkur and J. Lewinski, *Chem. Eur. J.*, 2012, **18**, 7367.

Chapter 2

Simple manual grinding synthesis of highly luminescent mononuclear Cu(I)-Iodide complexes

2-1 Introduction

Luminescent copper(I) complexes have attracted much attention because of their potential application for solar energy conversion,[1] luminescence based sensors,[2] and organic light-emitting diodes (OLEDs).[3] Especially, copper(I)-halide complexes with N- or P-donor ligands have been extensively investigated because these complexes exhibit strong luminescence[4] and interesting chromic properties such as thermochromic,[5] mechanochromic,[6] vapochromic,[7] and photochromic luminescence.[8]

Most luminescent Cu(I) complexes have been synthesized in organic solvents as ordinary ways. However, it is desirable to achieve the synthesis without organic solvents because the solvent-free synthesis can reduce environmental contamination and even be more convenient than the normal solvent-based synthesis. Mechanical synthesis using the hand grinding or the mechanical milling have been applied to synthesize metal complexes, organic compounds, coordination polymers (MOFs) and so on.[9] Mechanochemical syntheses are noted for their convenience and in many cases, for the short reaction time relative to the solution reactions. For example, the yield of $[CuI(etu)_2]_3$ (etu = ethylenethiourea) by the mechanochemical synthesis is higher (99 %) than that of the solution synthesis (50%).[10] In another instance, luminescent coordination polymers $[Cu_4I_4(bpmp)_m]_n$ (bpmp = 1,4-bis(pyridin-4-ylmethyl)piperadine, m = 2, 3) were obtained by the grinding syntheses in higher yield (80–84%) compared to solvothermal syntheses (62–65%).[11] In addition, the reaction time of grinding syntheses (40 min) was shorter than that of solvothermal syntheses (50 h). However, reports of the grinding synthesis to obtain strongly luminescent Cu(I) complexes are still very few.

In this chapter, the synthesis of highly luminescent mononuclear copper(I)-iodide complexes, $[CuI(PPh_3)_2(L)]$ (L = isoquinoline (iq) (**I-iq**), 1,6-naphthyridine (nap) (**I-nap**), pyridine (py) (**I-py**), Scheme 2-1) by simple manual grinding of Cu(I) iodide, PPh_3, and the L ligands were demonstrated.

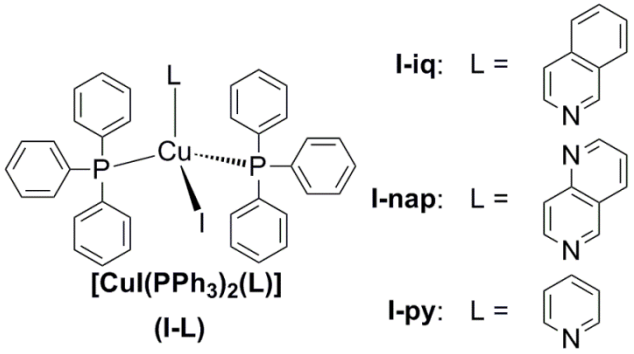

Scheme 2-1. Structure of $[CuI(PPh_3)_2(L)]$ (**I-L**).

2-2 Experimental

2-2-1 Materials and synthesis

All commercially available starting materials were used as received and solvents were used without any purification. Unless otherwise stated, all manipulations were conducted in air.

[CuI(PPh_3)$_2$(iq)] (I-iq) (iq = isoquinoline)

Preparation of single crystals

To a suspension of CuI (48.2 mg, 0.25 mmol) in iq (1 mL) was added PPh_3 (132 mg, 0.50 mmol). $CHCl_3$ (2 mL) was added to the reaction mixture. Yellow crystals were obtained by slow diffusion of diethyl ether vapor into the solution overnight. Yield. 174 mg, 83%. Elemental analysis calculated for $C_{45}H_{37}ICuNP_2$: C, 64.02; H, 4.42; N, 1.66. Found: C, 63.71; H, 4.40; N, 1.60.

Manual grinding synthesis (Method A)

CuI (0.5 mmol), PPh_3 (1.0 mmol) and iq (1.5 (3 eq), 2.5 (5 eq) or 5.0 (10 eq) mmol) were put in a mortar. The solids were ground together with a pestle for a few minutes. Et_2O was added to obtained yellow solid to remove unreacted ligands and impurity. The pale yellow solid was collected by filtration, washed with Et_2O, and dried in air. The PXRD patterns of the pale yellow solid are consistent with the simulated pattern based on the single crystal of **I-iq**. Yield, 85, 93 or 86% for 3, 5, 10 eq, respectively.

[CuI(PPh_3)$_2$(nap)] (I-nap) (nap = 1,6-naphthyridine)

Preparation of single crystal

To [CuI(PPh_3)$_3$] (63.3 mg, 0.065 mmol) was added a $CHCl_3$ solution (1 mL) of nap (101 mg, 0.77 mmol). Yellow crystals were obtained by slow diffusion of diethyl ether vapor into the solution overnight. Yield. 31.1 mg, 57%. Elemental analysis calculated for $C_{44}H_{36}ICuN_2P_2$: C, 62.53; H, 4.29; N, 3.31. Found: C, 62.24; H, 4.28; N, 3.30.

Manual grinding synthesis

CuI (0.25 mmol), PPh_3 (0.5 mmol) and nap (0.75 mmol) were put in a mortar and ground together with a pestle for a few minutes. Et_2O was added to the yellow solid to remove unreacted ligands and impurity. The yellow solid was colected by filtration, washed with Et_2O, and dried in air. The PXRD patterns of the white solids are consistent with the simulated pattern based on the single crystal of **I-nap**. Yield, 63%.

[CuI(PPh_3)$_2$(py)] (I-py) (py = pyridine)

Manual grinding synthesis (Method B)

CuI (0.5 mmol), py (10.0 mmol) were put in a mortar and ground together with a pestle for a few minutes. The reaction mixture was ground with PPh_3 (1.5 mmol) for additional several minutes. Et_2O were added to the white solid to remove unreacted ligands and impurity. The white solid was collected by filtration, washed with Et_2O, and dried in air. The PXRD patterns of the white solids are consistent with the simulated pattern based on the single crystal of **I-py**.[12] Yield, 81%.

2-2-2 Luminescence properties

The luminescence spectrum of each sample was measured using a JASCO FR-6600 spectrofluorometer at room temperature. The slit widths of the excitation and emission light were 5 and 6 nm, respectively. The luminescence quantum yield was recorded on a Hamamatsu Photonics C9920-02 absolute photoluminescence quantum yield measurement system equipped with an integrating sphere apparatus and 150-W CW xenon light source. Emission life time measurements were conducted by using Hamamatsu Photonics C4334 equipped with a streak camera as a photo detector at 337 nm excitation.

2-2-3 Single-crystal X-ray diffraction measurements

All single-crystal X-ray diffraction measurements were conducted using a Rigaku Mercury CCD diffractometer with graphite monochromated Mo Kα radiation (λ = 0.71069 Å) and a rotating anode generator. Each single-crystal was mounted on a MicroMount using paraffin oil. The crystal was then cooled using an N_2-flow type temperature controller. Diffraction data were collected and processed using the CrystalClear softwere.[13] Structures were solved by the direct method using SIR-2004[14] for **I-iq** and SIR-97[15] for **I-nap**. Structural refinements were conducted by the full-matrix least-squares method using SHELXL-97.[16] Non-hydrogen atoms were refined anisotropically, and hydrogen atoms were refined using the riding model. All calculations were conducted using the Crystal Structure crystallographic software package.[17] Crystallographic data obtained for each complex are summarized in Table 2-1.

Table 2-1. Crystal parameters and refinement data.

	I-iq	**I-nap**
T / K	200 (1)	200 (1)
Formula	$C_{45}H_{37}ICuNP_2$	$C_{44}H_{36}ICuN_2P_2$
Formula weight	844.19	845.18
Crystal system	Monoclinic	Monoclinic
Space group	$P2_1/c$	$P2_1/n$
a / Å	10.313(3)	9.9705(7)
b / Å	18.345(5)	35.823(2)
c / Å	20.464(5)	11.5829(7)
α / °	90	90
β / °	93.496(3)	114.770(2)
γ / °	90	90
V / Å ^{3}	3864.3(16)	3756.5(4)
Z	4	4
D_{cal} / g cm^{-3}	1.296	1.494
Reflections collected	27817	23121
Unique reflections	8328	8355
R_{int}	0.0450	0.0425
GOF	1.109	1.193
R_1 ($I > 2\sigma(I)$) [a]	0.0541	0.0358
wR_2 [b]	0.1450	0.0864

[a] $R_1 = \Sigma||F_o| - |F_c||/\Sigma|F_o|$. [b] $wR_2 = [\Sigma w(F_o^2 - F_c^2)/\Sigma w(F_o)^2]^{1/2}$, $w = [\sigma_c^2(F_o^2) + (xP)^2 + yP]^{-1}$, $P = (F_o^2 - 2F_c^2)/3$.

2-2-4 Powder X-ray diffraction measurements

Powder X-ray diffraction was conducted using a Bruker D8 Advance diffractometer equipped with a graphite monochlometer using Cukα radiation and one-dimensional LinxEye detector.

2-2-5 Theoretical Calculations

DFT calculations were performed with B3LYP functional[18] and the LANL2DZ basis[19] set using Gaussian 03 program.[20] Molecular structures determined by X-ray crystallographic analysis were used. Molecular orbital are shown using Avogadro 1.10.[21]

2-3 Results and discussion

2-3-1 Manual grinding synthesis of mononuclear Cu(I) complexes

Figure 2-1 shows the grinding synthesis of **I-iq**. By the grinding of CuI and PPh_3 with 3 eq of isoquinoline in an agate mortar using a pestle, the sample began to emit greenish-yellow luminescence at room temperature (Figure 2-1(d)) and within a few minutes, it exhibited intense luminescence under the UV light (Method A, Figure 2-1(f)). The powder X-ray diffraction (PXRD) pattern of pale yellow powder is almost identical to that of unwashed sample and totally different to that of CuI or PPh_3 (Figure 2-2). These results clearly show that the luminescent compound was formed not in the Et_2O solvent in the washing process, but by grinding (not adding Et_2O).

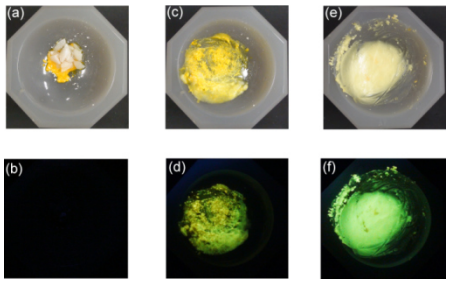

Figure 2-1. Bright field and luminescence images showing synthetic process of **I-iq** by the grinding method: (a, b) mixture of CuI, PPh_3 and iq before grinding, (c, d) the ground mixture after 8 s, (e, f) the ground mixture after 2 min.

In order to identify the strongly luminescent compound, single crystals of **I-iq** were prepared by the slow diffusion of diethyl ether to a chloroform solution including CuI, PPh_3 and excess amounts of iq. Single-crystal X-ray diffraction (SXRD) measurement revealed the mononuclear structure of **I-iq** which took the tetrahedral coordination geometry occupied by one iodide, one N atom of iq and two P atoms of PPh_3 ligand (Figure 2-3). Interestingly, the PXRD pattern of the strongly luminescent yellow solid obtained by the manual grinding is almost consistent with the simulated pattern calculated from the SXRD data of **I-iq**, indicating that the mononuclear Cu(I) complex **I-iq** can be synthesized easily in high yield without any impurities by the simple-grinding method (Figures 2-4(c) and 2-4(d)). These results suggest that the amount of the iq ligand was an important factor in the grinding synthesis. When CuI and PPh_3 were ground in the presence of 3 eq or more of iq, **I-iq** was obtained in excellent yields of 85–93% (Table 2-2, entries 3–5), whereas the reactions with less than 3 eq of iq led to the contamination of unreacted CuI as detected by PXRD (Figures 2-4(a) and 2-4(b)).

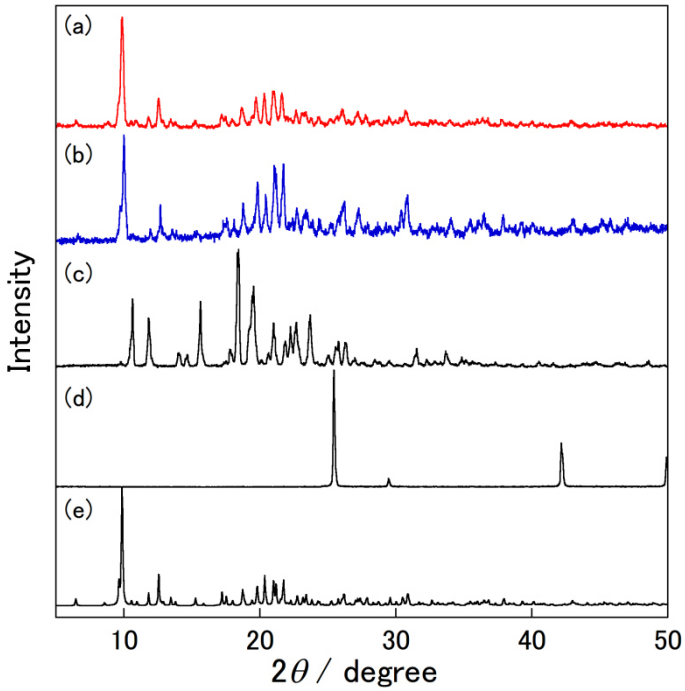

Figure 2-2. PXRD patterns of the pale yellow powder (a), unwashed sample (b), PPh_3 (c) and CuI (d) and the simulation pattern of **I-iq** (e).

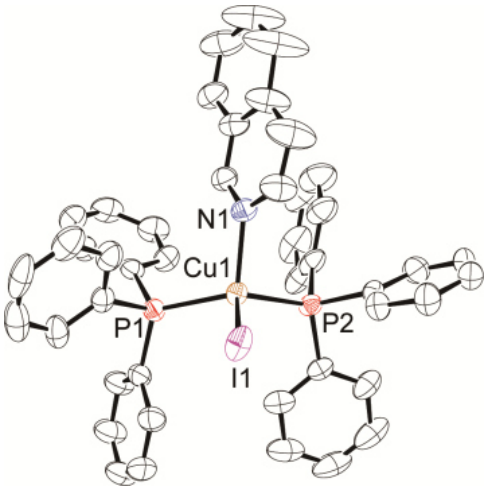

Figure 2-3. ORTEP drawing of **I-iq**. Hydrogen atoms are omitted for clarity. Displacement parameters are drawn at 50% probability level.

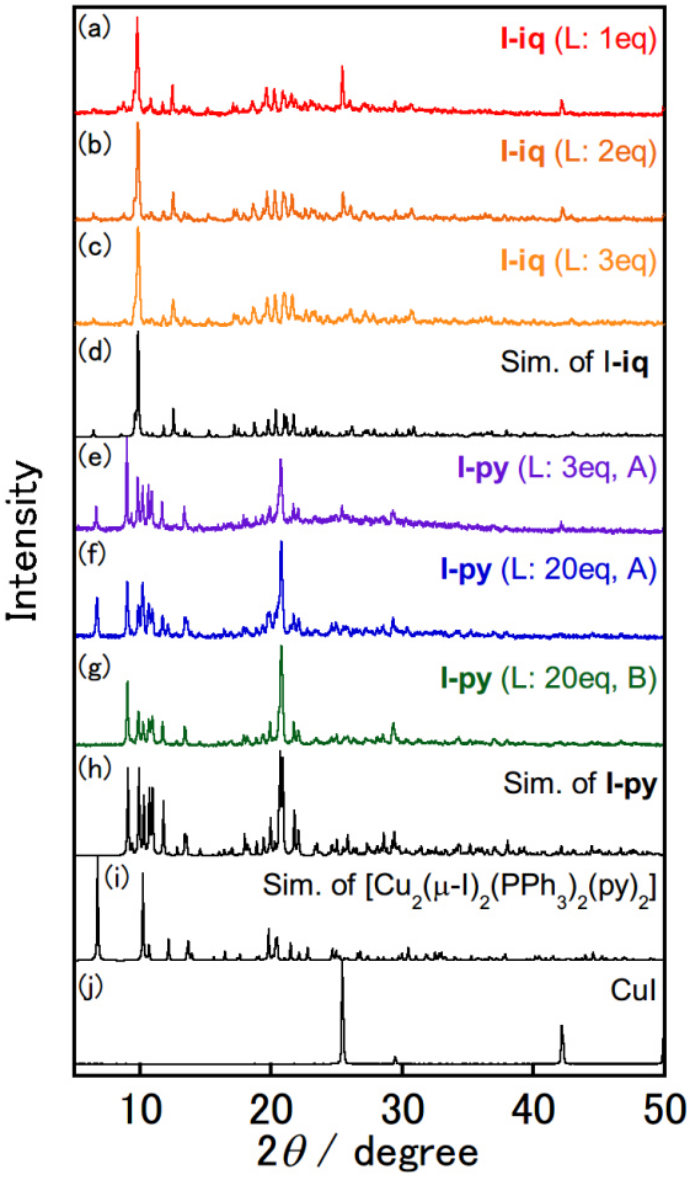

Figure 2-4. PXRD patterns of the samples prepared by the grinding methods in the different conditions; (a)–(c) for **I-iq** and (e)–(g) for **I-py** with the simulation patterns of (d) **I-iq**, (h) **I-py**[12a] and (i) $[Cu_2(\mu\text{-}I)_2(PPh_3)_2(py)_2]$[12b] and (j) the PXRD pattern of CuI.

To achieve the grinding synthesis of other luminescent mononulcear Cu(I) complexes bearing N-heteroaromatic ligands, the N-heteroaromatic ligand were changed from iq to nap or py for **I-nap** or **I-py**, respectively. When CuI and PPh_3 were ground with 3 eq of nap which has almost the same molecular shape of iq, **I-nap** was also successfully obtained in good yield without any impurities, which was confirmed by the SXRD and PXRD measurements (Table 2-2 entry 6, see Figures 2-5 and 2-6). In the case of py, however, the mixture of **I-py**, unreacted CuI and the dinuclear Cu(I) complex $[Cu_2(\mu\text{-}I)_2(PPh_3)_2(py)_2]$ was produced (Figure 2-4(e)) by the simple grinding of CuI, PPh_3 and 3 eq of py ligand. The increase in the amount of py (20 eq) was found to be effective to reduce the unreacted CuI, but the dinuclear complex was still formed (Figure 2-4(f)). Stepwise synthesis was found to be favorable for the preparation of mononuclear complex **I-py**: First, CuI was ground with 20 eq of py for a few minutes, and then 3 eq of PPh_3 was added to the mixture and ground for additional several minutes (Method B). The PXRD pattern of the product is consistent with the simulated pattern based on the single crystal diffraction of **I-py** (Figures 2-4(g) and 2-4(h)) indicating that **I-py** was purely synthesized by the stepwise grinding method.

The different reactivity in the grinding synthesis might be related with the difference in the viscosity of L. As iq and nap have the melting points at around room temperature (mp = 28°C for iq, 25–35°C for nap), they act as viscous oil in the grinding reactions (η (viscosity) = 3.2 mPa·s at 30°C for iq).[22] In that situation, thermal effect by grinding would be expected. On the other hand, py is fluid liquid with low viscosity (η = 0.88 mPa·s at 25°C, mp = –46°C). Thus pyridine can play a role of a good solvent which can promote the formation of the mononuclear and dinuclear complexes in equilibrium. To suppress the dimerization, the stepwise grinding synthesis (Method B) is effective probably because of the formation of an intermediate mononuclear complex, $[CuI(py)_3]$.

Table 2-2. Conditions for the grinding synthesis using CuI, PPh_3 and the L ligands.

Entry	Product	Method [a]	PPh_3 (eq)[b]	L (eq)[b]	Yield (%)
1	**I-iq**	A	2	1	-[c]
2	**I-iq**	A	2	2	-[c]
3	**I-iq**	A	2	3	85
4	**I-iq**	A	2	5	93
5	**I-iq**	A	2	10	86
6	**I-nap**	A	2	3	63
7	**I-py**	A	2	3	-[d]
8	**I-py**	A	2	20	-[d]
9	**I-py**	B	3	20	81

[a] Method A: the simple grinding of CuI and PPh_3 with L. Method B: the stepwise grinding of CuI and L followed by the addition of PPh_3. [b] equivalent amounts relative to CuI. [c] not measured because of the contamination of unreacted CuI. [d] not measured because of the contamination of unreacted CuI and/or $[Cu_2(\mu\text{-}I)_2(PPh_3)_2(py)_2]$.

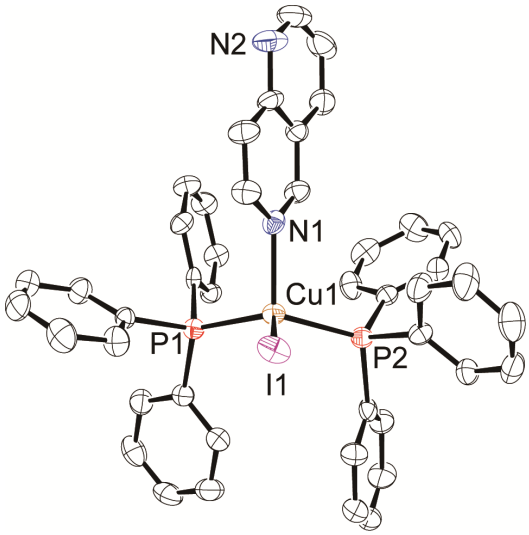

Figure 2-5. ORTEP drawing of **I-nap**. Hydrogen atoms are omitted for clarity. Displacement parameters are drawn at 50% probability level.

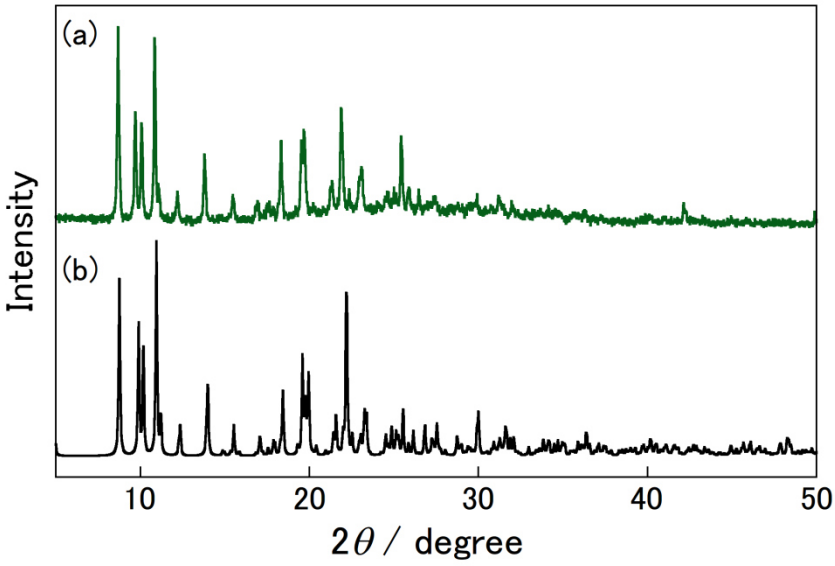

Figure 2-6. PXRD patterns of **I-nap** prepared by grinding method with 3 eq (a) and the simulation patterns of **I-nap** (b).

2-3-2 Luminescent properties

These complexes **I-iq**, **I-nap** and **I-py** exhibit strong emission in the solid states upon UV light irradiation. Figure 2-7 shows the emission spectra of **I-iq**, **I-nap** and **I-py**. Any samples prepared by crystallization and grinding syntheses gave essentially the same emission spectra. These are broad spectra without vibronic progressions, suggesting that the emissive excited states have the charge-transfer (CT) character. The difference in emission wavelength (λ_{max} = 535, 571, and 485 nm for **I-iq**, **I-nap** and **I-py**, respectively) also suggest that the emission states would be related to the π-conjugation of the L ligands. The photoluminescence quantum yields and the lifetimes at 298 K are summarized with the emission maxima in Table 2-3. Notably, these complexes exhibit high luminescence quantum yields of 0.63-0.99.

Table 2-3. Luminescence properties of **I-iq**, **I-nap** and **I-py** in the solid states at 298K.

compound	**I-iq**	**I-nap**	**I-py**
λ_{max}[a] / nm	535	571	485
τ / μs (A_n)[b]	27 (0.54),	4.7 (0.88)	10 (0.21),
	77(0.52)	6.6 (0.13)	20 (0.82)
Φ[c]	0.63	0.73	0.99

[a] Emission maxima. [b] Emission lifetime. The emission decay curves were analysed with two components ($I = A_1\exp(-t/\tau_s)+A_2\exp(-t/\tau_2)$). [c] Photoluminescence quantum yield in the solid states.

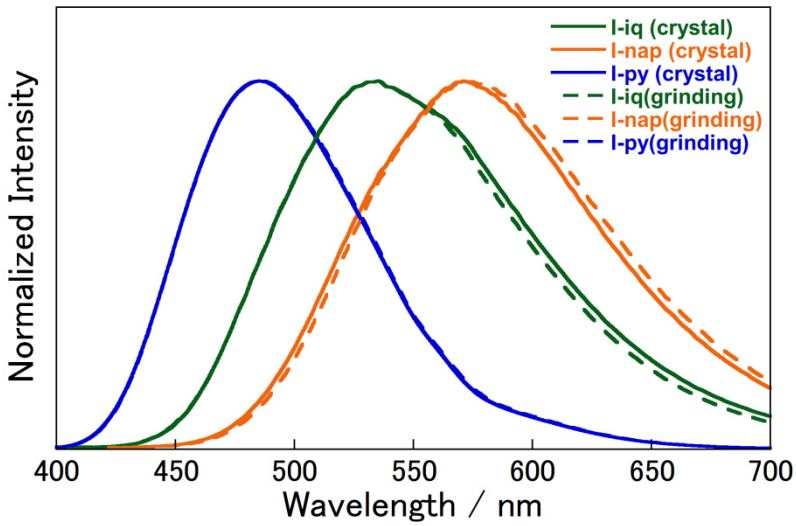

Figure 2-7. Luminescence spectra of **I-Iq**, **I-nap**, **I-py** in the crystals (solid line) and grinding sample (dotted line) (λ_{ex} = 370 nm (**I-iq**), 400 nm (**I-nap**), 350 nm (**I-py**)) at 298 K.

2-3-3 Theoretical calculations

To reveal the emissive excited states of **I-iq**, **I-nap** and **I-py**, time dependent-density functional theory (TD-DFT) calculations were carried out for **I-iq**, **I-nap** and **I-py** using the atomic coordinates determined by X-ray crystallographic analysis. Figure 2-8 shows molecular orbitals of complexes **I-iq**, **I-nap** and **I-py**. For all complexes, the electron density in the highest-occupied molecular orbital (HOMO) is distributed over the copper and iodine atoms, while that in the lowest-unoccupied molecular orbital (LUMO) is localized on the L ligands. These results suggests that the lowest excited states of **I-iq**, **I-nap** and **I-py** are combined metal-to-ligand charge transfer (MLCT) and halide-to-ligand charge transfer (XLCT) states ((M+X)LCT).

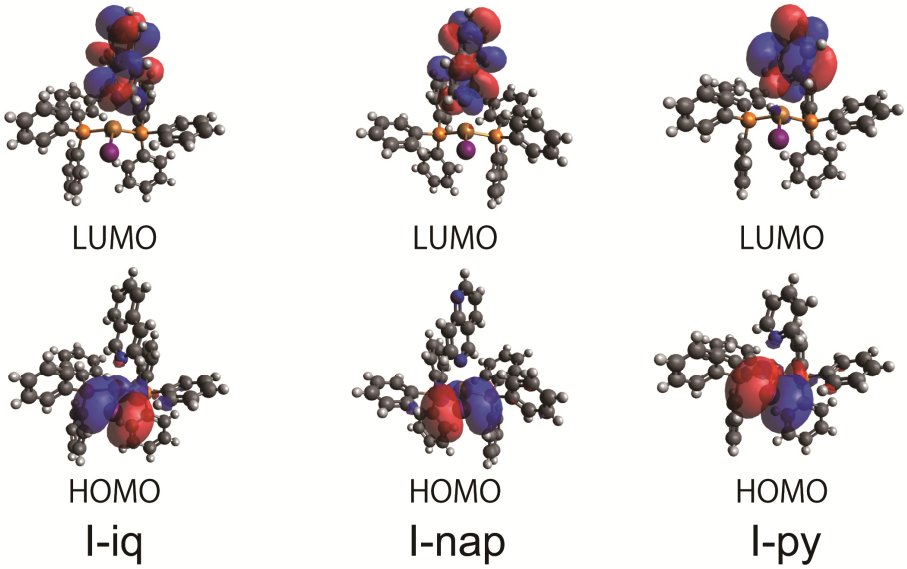

Figure 2-8. Molecular orbitals of complexes **I-iq, I-nap** and **I-py**.

2-4 Conclusion

Highly luminescent mononuclear copper(I)-iodide complexes were synthesized by the simple manual grinding of the materials. By the adjustment of the amount and timing of ligands, the grinding synthesis can be a useful and convenient method for luminescent mononuclear copper(I)-iodide complexes. These complexes exhibit strong emission with high photoluminescence quantum yield of 0.63-0.99 and their emission color depends on π-conjugation of L ligands. Such an efficient synthesis of desired strong emitters should be one of the important factors for their applications.

2-5 References

1 (a) S. P. Luo, E. Mejia, A. Friedrich, A. Pazidis, H. Junge, A. E. Surkus, R. Jackstell, S. Denurra, S. Gladiali, S. Lochbrunner and M. Beller, *Angew. Chem. Int. Ed.*, 2013, **52**, 419; (b) R. S. Khnayzer, C. E. McCusker, B. S. Olaiya and F. N. Castellano, *J. Am. Chem. Soc.*, 2013, **135**, 14068.

2 (a) C. S. Smith and K. R. Mann, *J. Am. Chem. Soc.*, 2012, **134**, 8786; (b) C. S. Smith, C. W. Branham, B. J. Marquardt and K. R. Mann, *J. Am. Chem. Soc.*, 2010, **132**, 14079.

3 (a) J. C. Deaton, S. C. Switalski, D. Y. Kondakov, R. H. Young, T. D. Pawlik, D. J. Giesen, S. B. Harkins, A. J. Miller, S. F. Mickenberg and J. C. Peters, *J. Am. Chem. Soc.*, 2010, **132**, 9499; (b) M. Hashimoto, S. Igawa, M. Yashima, I. Kawata, M. Hoshino and M. Osawa, *J. Am. Chem. Soc.*, 2011, **133**, 10348; c) S. Igawa, M. Hashimoto, I. Kawata, M. Yashima, M. Hoshino and M. Osawa, *J. Mater. Chem. C*, 2013, **1**, 542.

4 (a) H. Araki, K. Tsuge, Y. Sasaki, S. Ishizaka and N. Kitamura, *Inorg. Chem.*, 2005, **44**, 9667; (b) D. M. Zink, M. Bachle, T. Baumann, M. Nieger, M. Kuhn, C. Wang, W. Klopper, U. Monkowius, T. Hofbeck, H. Yersin and S. Bräse, *Inorg. Chem.*, 2013, **52**, 2292.

5 H. Kitagawa, Y. Ozawa and K. Toriumi, *Chem. Commun.*, 2010, **46**, 6302.

6 S. Perruchas, X. F. Le Goff, S. Maron, I. Maurin, F. Guillen, A. Garcia, T. Gacoin and J. P. Boilot, *J. Am. Chem. Soc.*, 2010, **132**, 10967.

7 X.-C. Shan, F.-L. Jiang, L. Chen, M.-Y. Wu, J. Pan, X.-Y. Wan and M.-C. Hong, *J. Mater. Chem. C*, 2013, **1**, 4339.

8 A. Kobayashi, K. Komatsu, H. Ohara, W. Kamada, Y. Chishina, K. Tsuge, H. -C. Chang and M. Kato, *Inorg. Chem.*, 2013, **52**, 13188.

9 (a) G. A. Bowmaker, *Chem. Commun.*, 2013, **49**, 334; (b) G. W. Wang, *Chem. Soc. Rev.*, 2013, **42**, 7668; (c) S. L. James, C. J. Adams, C. Bolm, D. Braga, P. Collier, T. Friscic, F. Grepioni, K. D. Harris, G. Hyett, W. Jones, A. Krebs, J. Mack, L. Maini, A. G. Orpen, I. P. Parkin, W. C. Shearouse, J. W. Steed and D. C. Waddell, *Chem. Soc. Rev.*, 2012, **41**, 413.

10 G. A. Bowmaker, J. V. Hanna, C. Pakawatchai, B. W. Skelton, Y. Thanyasirikul and A. H. White, *Inorg. Chem.*, 2009, **48**, 350.

11 S. Yuan, S.-S. Liu and D. Sun, *CrystEngComm*, 2014, **16**, 1927.

12 (a) L. M. Engelhardt, P. C. Healy, J. D. Kildea and A. H. White, *Aust. J. Chem.*, 1989, **42**, 895; (b) L. M. Engelhardt, P. C. Healy, J. D. Kildea and A. H. White, *Aust. J. Chem.*, 1989, **42**, 913.

13 *CrystalClear*, Molecular Structure Corporation, Orem, UT, 2001.

14 *SIR-2004*: M. C. Burla, R. Caliandro, M. Camalli, B. Carrozzini, G. L. Cascarano, L. De Caro, C. Giacovazzo, G. Polidori and R. Spagna, *J. Appl. Crystallogr.*, 2005, **38**, 381.

15 *SIR-97*: A. Altomare, M. C. Burla, M. Camalli, G. L. Cascarano, C. Giacovazzo, A. Guagliardi, A. G. Moliterni, G. Polidori and R. Spagna, *J. Appl. Crystallogr.*, 1999, **32**, 115.

16 *SHELXL-97*: G. M. Sheldrick, *Acta Crystallogr., Sect. A:Fundam. Crystallogr.,* 2008, **64**, 112.

17 *CrystalStructure 4.0*: Rigaku Corporation, Tokyo, Japan, 2000-2010.

18 (a) A. D. Becke, *J. Chem. Phys.*, 1993, **98**, 5648; (b) C. Lee, W. Yang and R. G. Parr, *Phys. Rev. B*, 1988, **37**, 785.

19 (a) P. J. Hay and W. R. Wadt, *J. Chem. Phys.*, 1985, **82**, 270; (b) W. R. Wadt and P. J. Hay, *J. Chem. Phys.*, 1985, **82**, 284; (c) P. J. Hay and W. R. Wadt, *J. Chem. Phys.*, 1985, **82**, 299.

20 M. J. Frisch, G. W. Trucks, H. B. Schlegel, G. E. Scuseria, M. A. Robb, J. R. Cheeseman, J. A. Montgomery, Jr., T. Vreven, K. N. Kudin, J. C. Burant, J. M. Millam, S. S. Iyengar, J. Tomasi, V. Barone, B. Mennucci, M. Cossi, G. Scalmani, N. Rega, G. A. Petersson, H. Nakatsuji, M. Hada, M. Ehara, K. Toyota, R. Fukuda, J. Hasegawa, M. Ishida, T. Nakajima, Y. Honda, O. Kitao, H. Nakai, M. Klene, X. Li, J. E. Knox, H. P. Hratchian, J. B. Cross, C. Adamo, J. Jaramillo, R. Gomperts, R. E. Stratmann, O. Yazyev, A. J. Austin, R. Cammi, C. Pomelli, J. W. Ochterski, P. Y. Ayala, K. Morokuma, G. A. Voth, P. Salvador, J. J. Dannenberg, V. G. Zakrzewski, S. Dapprich, A. D. Daniels, M. C. Strain, O. Farkas, D. K. Malick, A. D. Rabuck, K. Raghavachari, J. B. Foresman, J. V. Ortiz, Q. Cui, A. G. Baboul, S. Clifford, J. Cioslowski, B. B. Stefanov, G. Liu, A. Liashenko, P. Piskorz, I. Komaromi, R. L. Martin, D. J. Fox, T. Keith, M. A. Al-Laham, C. Y. Peng, A. Nanayakkara, M. Challacombe, P. M. W. Gill, B. Johnson, W. Chen, M. W. Wong, C. Gonzalez and J. A. Pople, *Gaussian 03 (Revision E.01)*, Gaussian, Inc., Wallingford CT, 2004.

21 M. D. Hanwell, D. E. Curtis, D. C. Lonie, T. Vandermeersch, E. Zurek and G. R. Hutchison, *J. Cheminform.*, 2012, **4**, 17.

22 H. Freise and W. L. Glowacki, *J. Am. Chem. Soc.*, 1949, **71**, 514.

Chapter 3

Simple and extremely efficient blue emitters based on mononuclear Cu(I)-halide complexes with delayed fluorescence

3-1 Introduction

Phosphorescent materials based on noble metal complexes, such as Ir(III) and Pt(II) complexes, have been increasingly developed for efficient light generation in organic light-emitting diodes (OLEDs).[1] Phosphorescent materials are advantageous over fluorescent materials because of their ability to harvest both singlet and triplet excitons, resulting in theoretically 100% internal quantum efficiency.[2] However, these phosphorescent materials are expensive and highly limited resources. Therefore, alternative materials are being developed.

Recently, thermally activated delayed fluorescence (TADF) materials based on non-noble metal complexes and organic compounds have attracted much attention because they can harvest both singlet and triplet excitons.[3] When the energy difference (ΔE) between the lowest excited singlet state (S_1) and the lowest excited triplet state (T_1) is small, the singlet state can be thermally activated at the expense of the triplet state. This strategy is particularly useful for efficient electroluminescent (EL) devices.[3a, b, 4] In this context, various types of TADF materials have been investigated. However, highly efficient blue-light-emitting TADF materials are still very few.[5] Zhang et al. reported efficient TADF organic compounds for blue light emission with the quantum yield, Φ = ~0.69, in toluene solution.[5a] On the other hand, Yersin and co-workers reported strong blue-luminescent Cu(I) complexes, [Cu(pop)(NN)] (pop = bis(2-(diphenyl-phosphanyl)phenyl)ether, NN = bidentate pyrazolylborate, Φ = ~0.90 in powder) and $[Cu_2(\mu\text{-}X)_2(PN)_2]$ (PN = aminophosphane ligands, Φ = ~0.65 in powder), in which emissions were assigned to TADF.[5b, c] Cu(I) complexes with tetrahedral geometry have great potential for the synthesis of efficient TADF materials because of the small ΔE based on the metal-to-ligand charge transfer (MLCT) state, where the stability of the triplet state is small (<ca. 1000 cm^{-1}) owing to small exchange interactions. Thus, if a rigid structure that can suppress the deformation at the excited states is designed, Cu(I) complexes can be expected to exhibit strong luminescence based on TADF.[3b,c, 5b-d, 6] In particular, Cu(I)-halide complexes bearing N-heteroaromatic ligands can provide systematic emitters with different emission colors from red to blue, as observed for dinuclear complexes, $[Cu_2(\mu\text{-}X)_2(PPh_3)_2(L)_n]$ (L = N-heteroaromatic compounds, PPh_3 = triphenylphosphine), and $[Cu_2(\mu\text{-}X)_2(P\text{^}N)_3]$ (P^N = N-heteroaromatic compounds with a diphenylphosphino group), by systematic changes in the L and P^N ligands.[7] Therefore, the proper choice of N-heteroaromatic ligands is essential for the facile synthesis of strong blue luminescent materials. In this chapter, simple but strong luminescent blue light emitters based on mononuclear Cu(I)-halide complexes containing 4-methylpyridine (Mepy), $[CuX(PPh_3)_2(Mepy)]$ (X = Cl^- (**Cl-Mepy**), Br^- (**Br-Mepy**), and I^- (**I-Mepy**); Scheme 3-1) were discussed. The blue emission of these complexes

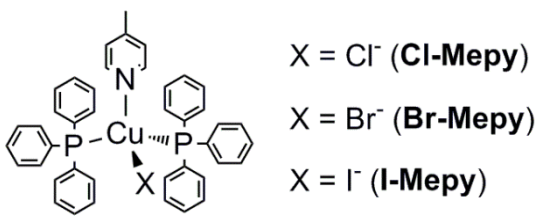

Scheme 3-1. Structure of $[CuX(PPh_3)_2(Mepy)]$.

was derived from TADF with the photoluminescence quantum yields approaching 100% (for **Cl-Mepy** and **Br-Mepy**) in the crystals at room temperature. Notably, these complexes were prepared by easy and environmentally benign procedures.

3-2 Experimental

3-2-1 Materials and synthesis

All commercially available starting materials were used as received and solvents were used without any purification. Unless otherwise stated, all manipulations were conducted in air. $[CuCl(PPh_3)_3]\cdot CH_3CN$ was prepared according to the literature procedure.[8] The ^1H NMR spectrum of each sample was measured using a JEOL EX-270 NMR spectrometer at room temperature. Elemental analysis was conducted at the analysis centre at Hokkaido University.

$[CuCl(PPh_3)_2(Mepy)]$ (**Cl-Mepy**) To $[CuCl(PPh_3)_3]\cdot CH_3CN$ (88.7 mg, 0.096 mmol) was added Mepy (1 mL) and then $CHCl_3$ (1 mL). Colourless crystals were obtained by slow diffusion of diethyl ether vapour into the solution overnight. Yield. 39 mg, 56%. ^1H NMR (270 MHz, CHLOROFORM-d) δ ppm 2.24 (s, 3H) 7.19-7.43 (m, 34 H). Elemental analysis calculated for $C_{42}H_{37}ClCuNP_2$: C, 70.39; H, 5.20; N, 1.95. Found: C, 70.74; H, 5.30; N 1.91.

$[CuBr(PPh_3)_2(Mepy)]$(**Br-Mepy**) **Method 1.** To a suspension of CuBr (42.5 mg, 0.30 mmol) in Mepy (1 mL) was added PPh_3 (680 mg, 2.6 mmol). $CHCl_3$ (1 mL) was added to the reaction mixture and then filtered to remove precipitate. Colourless crystals were obtained by slow diffusion of diethyl ether vapour into the solution overnight. Yield. 110 mg, 47%. ^1H NMR (270 MHz, CHLOROFORM-d) δ ppm 2.34 (s, 3H) 7.09 (d, *J*=5.6 Hz, 2H) 7.17-7.45 (m, 30H) 8.47 (d, *J*=5.6 Hz, 2H), Elemental analysis calculated for $C_{42}H_{37}BrCuNP_2$: C, 66.27; H, 4.90; N, 1.84. Found: C, 66.17; H, 4.92; N 1.84. **Method 2.** CuBr (39.4 mg, 0.27 mmol), PPh_3 (136 mg, 0.52 mmol) and Mepy (0.24 mL, 2.5 mmol) were added to the mortar. The solids were ground together with the pestle with intermediate scraping of the mortar with a spatula. The white solids were added to Et_2O to remove the unreacted ligands and impurity. The white solids were collected by filtration, washed with Et_2O, and dried in air. The PXRD patterns of the white solids are consistent with the simulated pattern based on the single crystal of **Br-Mepy** (Figure 3-1). Yield. 102 mg, 49%.

$[CuI(PPh_3)_2(Mepy)]$ (**I-Mepy**) **Method 1.** To a suspension of CuI (48.9 mg, 0.26 mmol) in Mepy (1 mL) was added PPh_3 (660 mg, 2.5 mmol) and then $CHCl_3$ (1 mL). Colourless crystals were obtained by slow diffusion of diethyl ether vapour into the solution for 1 week. Yield. 177.1 mg, 85%. ^1H NMR (270 MHz, CHLOROFORM-d) δ ppm 2.34 (s, 3H) 7.08 (d, *J*=5.6 Hz, 2H) 7.17-7.47 (m, 30H) 8.43-8.50 (m, 2H). Elemental analysis calculated for $C_{42}H_{37}ICuNP_2$: C, 62.42; H, 4.61; N, 1.73. Found: C, 62.50; H, 4.63; N, 1.75. **Method 2.** CuI (49 mg, 0.26 mmol), PPh_3 (130 mg, 0.50 mmol) and Mepy (0.24 mL, 2.5 mmol) were added to the mortar. The solids were ground together with the pestle with intermediate scraping of the mortar with a spatula. The white solids were added to Et_2O

to remove the unreacted ligands and impurity. The white solids were collected by filtration, washed with Et_2O, and dried in air. The PXRD patterns of the white solids are consistent with the simulated pattern based on the single crystal of **I-Mepy** (Figure 3-1). Yield. 177 mg, 85%.

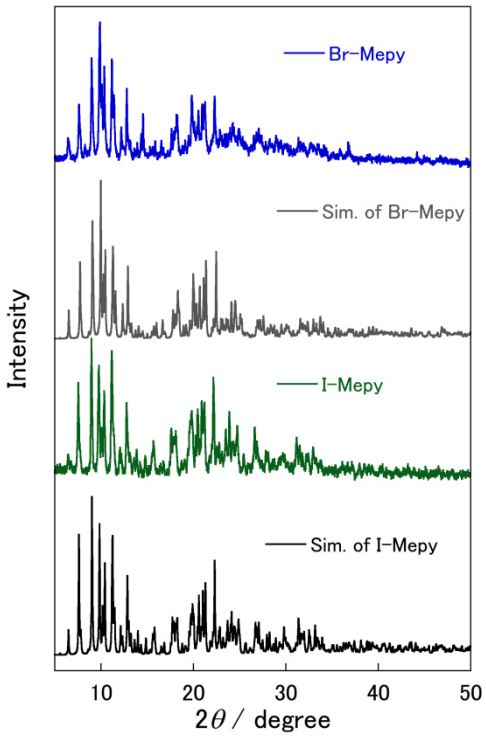

Figure 3-1. PXRD patterns of **Br-Mepy** and **I-Mepy** prepared by Method 2 and simulated diffraction pattern based on the single crystal structure of **Br-Mepy** and **I-Mepy**.

3-2-2 Luminescence measurement

The luminescence spectrum of each sample was measured using a JASCO FR-6600 spectrofluorometer at room temperature. The slit widths of the excitation and emission light were 5 and 6 nm, respectively. The luminescence quantum yield was recorded on a Hamamatsu Photonics C9920-02 absolute photoluminescence quantum yield measurement system equipped with an integrating sphere apparatus and 150-W CW xenon light source. Hamamatsu Photonics A10095-03 non-luminescent quartz sample holder was used for absolute photoluminescence quantum yield measurement. This quantum yield measurement was performed in air atmosphere; in order to verify the reliability and accuracy of our techniques, I determined the direct quantum yield of anthracene ethanol solution using this setup and attained the correct value of 0.27.[9] Emission life time measurements were conducted by using a streak camera equipped with Hamamatsu Photonics, C4334 as a photo detector at 337 nm excitation A liquid N_2 cryostat (Optistat-DN optical Dewar and ITC-503 temperature controller, Oxford Instruments) was used to control a sample temperature.

3-2-3 Single-crystal X-ray diffraction measurements

All single-crystal X-ray diffraction measurements were conducted using a Rigaku Mercury CCD diffractometer with graphite monochromated Mo Kα radiation (λ = 0.71069 Å) and a rotating anode generator. Each single-crystal was mounted on a MicroMount using paraffin oil. The crystal was then cooled using an N_2-flow type temperature controller. Diffraction data were collected and processed using the CrystalClear softwere.[10] Structures were solved by the direct method using SIR-2004[11] for **Cl-Mepy**, SIR-97[12] for **Br-Mepy** and SIR-2002[13] for **I-Mepy**. Structural refinements were conducted by the full-matrix least-squares method using SHELXL-97.[14] Non-hydrogen atoms were refined anisotropically, and hydrogen atoms were refined using the riding model. All calculations were conducted using the Crystal Structure crystallographic software package.[15] Crystallographic data obtained for each complex are summarized in Table 3-1.

3-2-4 Powder X-ray diffraction measurements

Powder X-ray diffraction was conducted using a Bruker D8 Advance diffractometer equipped with a graphite monochrometer using Cu-Kα radiation and one-dimensional LinxEye detector.

Table 3-1. Crystal parameters and refinement data.

	Cl-Mepy	**Br-Mepy**	**I-Mepy**
T / K	200 (1)	200 (1)	200 (1)
Formula	$C_{42}H_{37}ClCuNP_2$	$C_{42}H_{37}BrCuNP_2$	$C_{42}H_{37}ICuNP_2$
Formula weight	716.71	761.16	808.16
Crystal system	Monoclinic	Triclinic	Triclinic
Space group	$P2_1/n$	$P\ \bar{1}$	$P\ \bar{1}$
a / Å	9.973(3)	11.4725(6)	11.641(3)
b / Å	24.648(6)	16.0533(11)	16.112(5)
c / Å	15.235(4)	19.838(2)	19.967(6)
α / °	90	100.594(5)	100.657(5)
β / °	101.227(3)	93.054(4)	92.322(5)
γ / °	90	94.306(2)	94.296(3)
V / Å^3	3673(2)	3572.9(5)	3664(2)
Z	4	4	4
D_{cal} / g cm^{-3}	1.296	1.415	1.465
Reflections collected	28176	27989	53612
Unique reflections	8328	15717	16658
R_{int}	0.0500	0.0272	0.0511
GOF	1.091	1.070	1.134
R ($I > 2\sigma(I)$)	0.0456	0.0403	0.0556
Rw^a	0.1193	0.1042	0.1400

$^a R_W = [\Sigma(w(F_o^2 - F_c^2)^2)/\Sigma w(F_o^2)^2]^{1/2}$.

3-2-5 Theoretical Calculations

DFT calculations were performed with B3LYP functional[16] and the LANL2DZ basis[17] set using Gaussian 03 program.[18] Molecular structures determined by X-ray crystallographic analysis were used. Molecular orbital are shown using Avogadro 1.10.[19]

3-3 Results and discussion

3-3-1 Syntheses of mononuclear Cu(I) complexes

The mononuclear Cu(I) complex, **Cl-Mepy**, was synthesized simply by mixing [$CuCl(PPh_3)_3$] and Mepy in $CHCl_3$. Interestingly, **Br-Mepy** and **I-Mepy** were prepared from simple materials such as CuX (X = Br^-, I^-), PPh_3, and Mepy without using any solvent. After mixing CuX and PPh_3 with the ratio of 1:2 in a drop of Mepy (around 10 equimolar amounts), products were obtained that emitted blue luminescence under UV light (Method 2). The colourless block crystals of complexes **Cl-Mepy**, **Br-Mepy** and **I-Mepy** were produced by the slow diffusion of diethyl ether to $CHCl_3$ solutions including [$CuCl(PPh_3)_3$] andMepy or CuX (X = Br^-, I^-), PPh_3 and Mepy.

3-3-2 Crystal structures

Figure 3-2 shows the ORTEP drawings of **Cl-Mepy**, **Br-Mepy** and **I-Mepy**. X-ray crystallography revealed that **Cl-Mepy**, **Br-Mepy** and **I-Mepy** adopt a mononuclear tetrahedral coordination geometry occupied by one halide, one N atom of Mepy, and two P atoms of PPh_3 (Figure 3-2(a–e)). Only one crystallographically independent Cu(I) complex molecule was observed in **Cl-Mepy**, whereas two independent molecules were observed in **Br-Mepy** and **I-Mepy**. This is probably because of the steric hindrance of larger halides (Br^- and I^-) in **Br-Mepy** and **I-Mepy**. The torsion angle between the Mepy ring and Cu–X bond of **Cl-Mepy** (ca. 29°) is smaller than those of **Br-Mepy** and **I-Mepy** (47–53°). The two P atoms of **Cl-Mepy** are coordinated symmetrically with respect to the Cu–X bond, while those of **Br-Mepy** and **I-Mepy** are coordinated asymmetrically showing the relatively larger distortion (Table 3-2). These structural differences indicate that large halide ions such as Br^- and I^- caused steric repulsion between the two PPh_3 ligands, and this steric repulsion create a space to provide conformational flexibility to the Mepy ligand. Consequently, two independent molecules are allowed in the crystals of complexes **Br-Mepy** and **I-Mepy**.

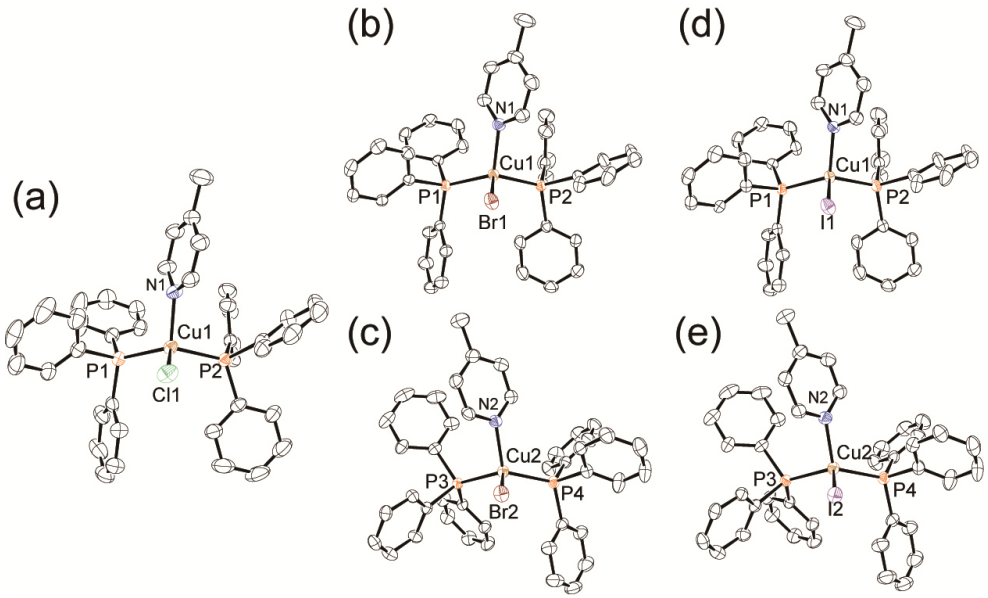

Figure 3-2. ORTEP drawings of (a) complex **Cl-Mepy**, (b) and (c) complex **Br-Mepy**, and (d) and (e) complex **I-Mepy**. Hydrogen atoms are omitted for clarity. Displacement parameters are drawn at 50% probability level.

Table 3-2. Selected bond length, torsion angles and bond angles of **Cl-Mepy**, **Br-Mepy** and **I-Mepy**.

	Cl-Mepy	**Br-Mepy**		**I-Mepy**	
		A	**B**	**A**	**B**
Cu-X / Å	2.3092(9)	2.4762(5)	2.4604(4)	2.6594(10)	2.6443(9)
Cu-N / Å	2.103(2)	2.119(2)	2.113(3)	2.119(4)	2.116(5)
Cu1(Cu2)-P1 (P3) / Å	2.2539(8)	2.2671(8)	2.2880(7)	2.2745(14)	2.3011(14)
Cu1(Cu2)-P2 (P4) / Å	2.2725(7)	2.2923(7)	2.2659(7)	2.2915(15)	2.2789(15)
X-Cu-N-C (Mepy) / °	29.00(13)	47.37(14)	-53.33(14)	46.7(3)	-53.0(3)
P1(P3)-Cu1 (Cu2)-X / °	106.04(3)	105.77(2)	111.610(19)	104.35(4)	110.63(4)
P2(P4)-Cu1 (Cu2)-X / °	107.11(3)	111.28(2)	104.29(3)	111.99(4)	103.99(4)

3-3-3 Luminescent properties

Cl-Mepy, **Br-Mepy** and **I-Mepy** crystals exhibit strong emission as shown in Figure 3-3. The luminescent measurement were performed with crystal samples due to the limited chemical stability in solution in analogue with other Cu(I)-halide complexes.[5c, 7a] Figure 3-4 shows the emission spectra at room temperature and 77 K. All the complexes, **Cl-Mepy**, **Br-Mepy** and **I-Mepy**, provide similar broad emission spectra without vibronic progression, indicating that the emissive excited states have a charge-transfer property. Each emission spectrum at 77 K shifted to lower energies by ca. 940–1230 cm^{-1} than that at room temperature. Regarding the effect of halide ligands, the emission spectra of **I-Mepy** appeared at shorter wavelength regions compared to those of **Cl-Mepy** and **Br-Mepy**, even though the difference is very small. A similar trend was observed for more commonly used halide-bridged dinuclear complexes.[3c, 5c, 7c]

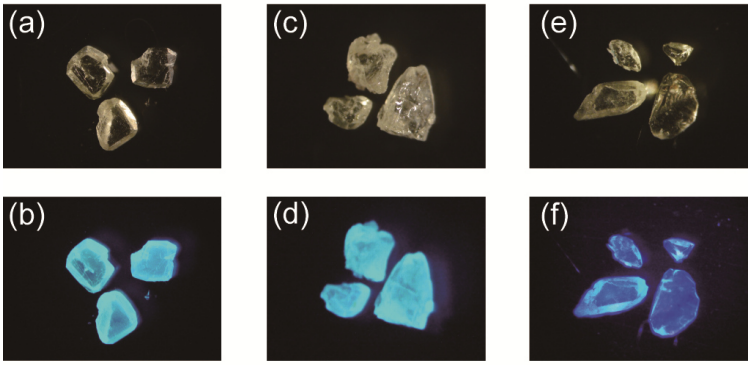

Figure 3-3. Photographs of crystals **Cl-Mepy** (a and b), **Br-Mepy** (c and d) and **I-Mepy** (e and f) under bright field and UV light, respectively.

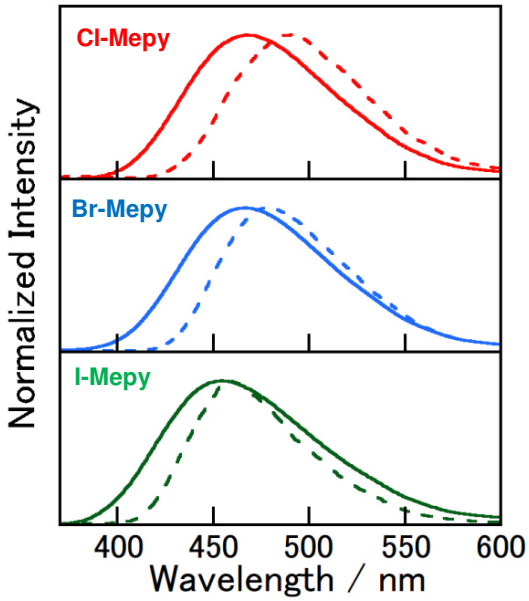

Figure 3-4. Luminescence spectra of **Cl-Mepy**, **Br-Mepy** and **I-Mepy** in the solid states (λ_{ex} = 350 nm) at room temperature (solid lines) and 77 K (dotted lines).

Along with the emission maxima, photoluminescence quantum yields and lifetimes at room temperature and at 77 K are listed in Table 3-3. Notably, these simple complexes exhibit very high quantum yields at room temperature (0.99 for **Cl-Mepy**, 0.95 for **Br-Mepy**, and 0.66 for **I-Mepy**, respectively). The emission lifetimes of **Cl-Mepy**, **Br-Mepy** and **I-Mepy** in the crystals were estimated by the least-square fitting of the emission decays using two exponentials, i.e., $I = A_1\exp(-t/\tau_1) + A_2\exp(-t/\tau_2)$, where τ_1 and τ_2 are the lifetimes, and A_1 and A_2 are the pre-exponential factors. Because the time-resolved emission spectra in the crystals are unchanged during the entire decay, the two decay components are considered to be the emission from different sites with the same electronic origin (Figure 3-5). The lifetimes of **Cl-Mepy**, **Br-Mepy** and **I-Mepy**, with the values ranging from several microseconds to several tens of microseconds at room temperature, are similar to those previously reported for Cu(I) complexes such as $[Cu_2(\mu\text{-}X)_2(PPh_3)_2\ (L)_n]$,[7a] whose luminescence was assigned to phosphorescence, and $[Cu_2(\mu\text{-}I)_2(dppb)_2]$ and $[CuI(dppb)PPh_3]$ (dppb = 1,2-bis[diphenylphosphino]-benzene), which showed delayed fluorescence at room temperature.[3c] Thus, the blue luminescence of **Cl-Mepy**, **Br-Mepy** and **I-Mepy** may have a similar origin. Then, the radiative rate constants (k_r) of **Cl-Mepy**, **Br-Mepy** and **I-Mepy** were estimated from the average emission lifetime (τ_{av}) by using equation (1)[20] for two exponential decay components:

$$\tau_{av} = \frac{A_1\tau_1^2 + A_2\tau_2^2}{A_1\tau_1 + A_2\tau_2} \qquad (1)$$

The τ_{av} of **Cl-Mepy**, **Br-Mepy** and **I-Mepy** and k_r, which was estimated by using the relation $k_r = \Phi/\tau_{av}$, and the nonradiative rate constants k_{nr} are also listed in Table 3-3. The results indicate that the radiative constants at 298 K are in a similar range (k_r = 6–11 × 10^4 s^{-1}), while a difference was observed in the nonradiative rate constants. Iodide complex **I-Mepy** has a much larger value (k_{nr} = 3.6 × 10^4 s^{-1}) than the others (k_{nr} = 1–3 × 10^3 s^{-1} for complexes **Cl-Mepy** and **Br-Mepy**). For all the complexes, the radiative constants at room temperature are several times larger than those at 77 K, indicating that the origins of the emissions at 298 and 77 K are different.

Table 3-3. Luminescence properties of complexes **Cl-Mepy**, **Br-Mepy** and **I-Mepy** in the solid states at 298 K and 77 K.

Compound	**Cl-Mepy**		**Br-Mepy**		**I-Mepy**	
	298 K	77 K	298 K	77 K	298 K	77 K
λ_{max} [a] (nm)	468	488	467	477	455	458
τ (μs (A_n)) [b]	5.8 (0.43)	18.3 (0.17)	9.6 (0.38)	41.0 (0.59)	3.9 (0.67)	46.1 (0.67)
	10.7 (0.64)	38.0 (0.82)	16.6 (0.72)	61.9 (0.47)	11.5 (0.52)	61.5 (0.36)
Φ [c]	0.99	0.82	0.95	0.95	0.66	0.76
τ_{av} [d] (μs)	9.4	36	15	52	9.5	52
k_r [e] (s^{-1})	1.1×10^5	2.3×10^4	6.3×10^4	1.8×10^4	6.9×10^4	1.4×10^4
k_{nr} [f] (s^{-1})	1.1×10^3	5.0×10^3	3.3×10^3	9.5×10^2	3.6×10^4	4.4×10^3

[a] Emission maximum. [b] Emission lifetime. Emission decays were analysed with two components: $I = A_1\exp(-t/\tau_1) + A_2\exp(-t/\tau_2)$. [c] Photoluminescence quantum yields in the solid states. [d] Average emission lifetimes were determined by using eq 1. [e] Radiative rate constants k_r were estimated by Φ/τ_{av}. [f] Nonradiative rate constants k_{nr} were estimated by $k_r(1 - \Phi)/\Phi$.

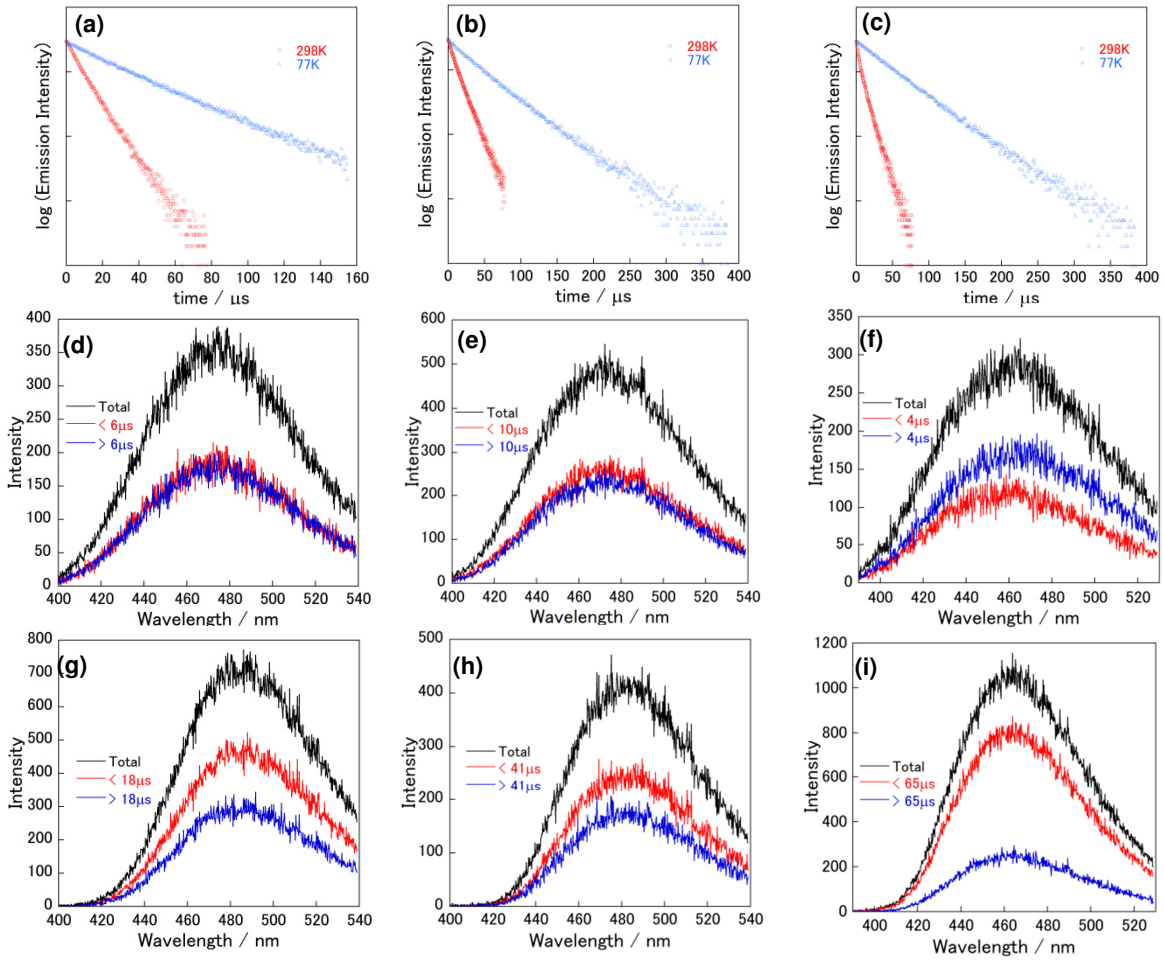

Figure 3-5. Emission decays of **Cl-Mepy** (a), **Br-Mepy** (b) and **I-Mepy** (c) in the solid states and time-resolved emission spectra of **Cl-Mepy**, **Br-Mepy** and **I-Mepy** at 298K (d, e, and f) and 77K (g, h, and i).

3-3-4 Emission lifetime analyses

To describe the two emission states quantitatively, temperature dependence of the average emission lifetimes of **Cl-Mepy**, **Br-Mepy** and **I-Mepy** was investigated (Figure 3-6). From 77 K to 170 K, the lifetimes changed gradually for all the complexes. However, at higher temperatures above 170 K, a sharp decrease in the lifetimes was observed. Assuming the two-state model involving the lowest excited singlet state (S_1) and the lowest excited triplet state (T_1), the observed lifetime can be expressed as a Boltzmann average by using equation (2).[4b, 5c, d, 6, 21]

$$\tau_{obs} = \frac{3+exp(-\Delta E/RT)}{3/\tau_{T_1}+1/\tau_{S_1}exp(-\Delta E/RT)} \qquad (2)$$

where, ΔE is the energy difference between the singlet and triplet states, τ_{S1} and τ_{T1} are the lifetimes of S_1 (fluorescence) and T_1 (phosphorescence) states, R is the ideal gas constant, and T is the absolute temperature. In this two-state model analysis, average lifetime was used instead of τ_{obs}, i.e., $\tau_{obs} = \tau_{av}$. The corresponding fitting parameters are listed in Table 3-4. The obtained ΔE values (940, 1070, and 1170 cm^{-1} for **Cl-Mepy**, **Br-Mepy** and **I-Mepy**, respectively) are roughly consistent to the spectral shifts of ~1000 cm^{-1} between 298 and 77 K, indicating that the two-state model is reasonable in the temperature region. The values are also comparable to those reported for several Cu(I) complexes.[3b,c, 4b, 5b-d, 6, 22] At room temperature, the emissions of **Cl-Mepy**, **Br-Mepy** and **I-Mepy** occur mainly from the singlet state by efficient up-conversion. Using fitting parameters, singlet components of luminescence ($I(S_1)/I_{total}$) can estimated by using equation (3) [5c]

$$\frac{I(S_1)}{I_{total}} = 1 - \left(1 + \frac{\Phi_{S1}\tau_{T1}}{3\Phi_{T1}\tau_{S1}} exp(-\Delta E/RT)\right)^{-1} \qquad (3)$$

where, Φ_{S1} and Φ_{T1} are luminescence quantum yields of the singlet and triplet states. We approximate Φ_{S1} and Φ_{T1} by Φ at 298K and 77K, respectively. The estimated singlet components at 298 K are 76%, 70% and 78% for **Cl-Mepy**, **Br-Mepy** and **I-Mepy**, respectively. The energy difference between the singlet and triplet states increases in the order of **Cl-Mepy**, **Br-Mepy** and **I-Mepy**. This is probably related to the lowering of the emission quantum efficiency of **I-Mepy** because a larger population in the triplet state with smaller rate constants (i.e., longer lifetime) should be affected by the nonradiative decay. Thus, **I-Mepy** with the largest ΔE has the lowest quantum efficiency (0.66 at 298 K) among the three complexes. On the other hand, almost 100% quantum yield is achieved by chloride complex **Cl-Mepy** with the smallest ΔE (940 cm^{-1}), even though the value is not so small compared to those reported (e.g., 460-630 cm^{-1} for $[Cu_2(\mu\text{-}X)_2(PN)_2]$).[5c] This proves the superior properties of these simple mononuclear complexes.

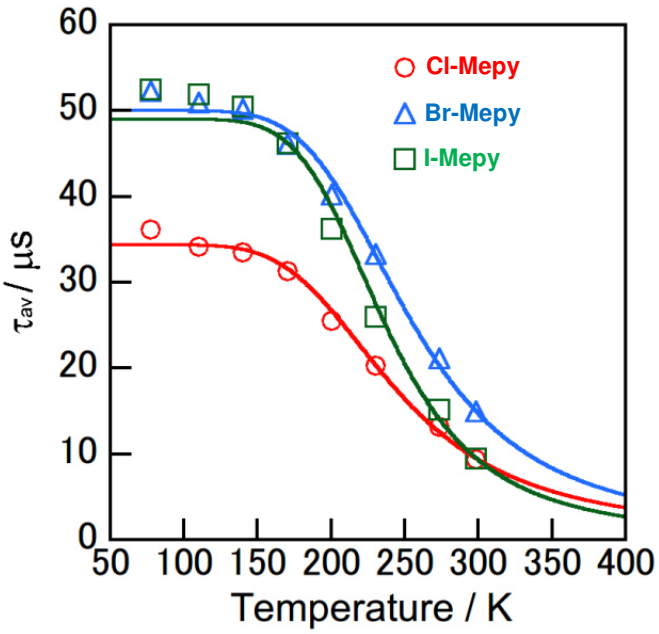

Figure 3-6. Temperature dependence of the average emission lifetimes of **Cl-Mepy**, **Br-Mepy** and **I-Mepy** in the solid states. The solid lines were calculated by using eq 2.

Table 3-4. Fitting parameters based on the two-state model (eq 2).

	Cl-Mepy	**Br-Mepy**	**I-Mepy**
ΔE [a]	940 cm^{-1}	1070 cm^{-1}	1170 cm^{-1}
$\tau(S_1)$ [b]	47 ns	41 ns	14 ns
$\tau(T_1)$ [b]	34 μs	50 μs	49 μs

[a] Energy difference between S_1 and T_1. [b] lifetimes of the S_1 and T_1 states determined by the fitting using eq 2 using the averaged emission lifetimes.

3-3-5 Theoretical calculations

To determine the emissive excited states of **Cl-Mepy**, **Br-Mepy** and **I-Mepy**, time dependent-density functional theory (TD-DFT) calculations were carried out for **Cl-Mepy**, **Br-Mepy** and **I-Mepy** using the atomic coordinates determined by X-ray crystallographic analysis (Figure 3-7). The electron density in the highest occupied molecular orbital (HOMO) and HOMO-1 are distributed over the Cu and halogen atom, while that in the lowest unoccupied molecular orbital (LUMO) is localized on the Mepy ligand. For **Br-Mepy** and **I-Mepy**, the HOMO-LUMO transition contributes to the lowest excited state by 100%. For complex **Cl-Mepy**, the HOMO-LUMO and HOMO-1 and LUMO transition are contribute to the lowest excited state by 26 and 74%, respectively. Thus, the lowest excited states of complexes **Cl-Mepy**, **Br-Mepy** and **I-Mepy** are combined MLCT and halide-to-ligand charge transfer (XLCT) states, ((M+X)LCT).

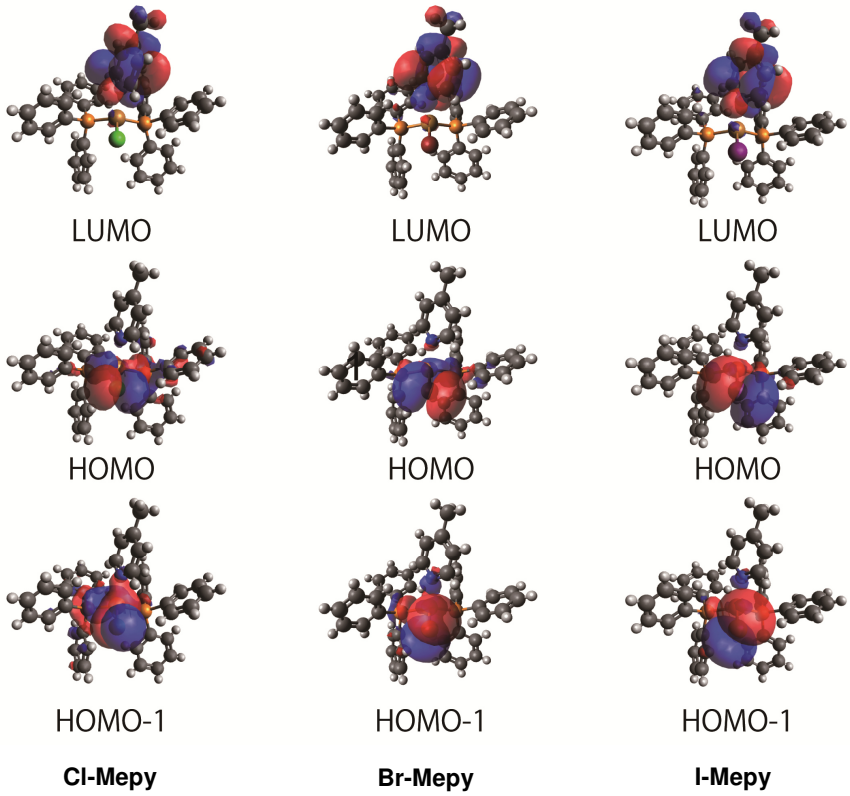

Figure 3-7. Molecular orbitals of **Cl-Mepy**, **Br-Mepy** and **I-Mepy.**

3-3-6 Possible mechanism of luminescence

Scheme 3-2 shows the schematic luminescent mechanism diagram of **Cl-Mepy**, **Br-Mepy** and **I-Mepy**. At room temperature, the ^{1}(M+X)LCT state is easily thermally accessible from the ^{3}(M+X)LCT emissive state because of the small ΔE (940–1170 cm^{-1}). Thus, all the complexes, **Cl-Mepy**, **Br-Mepy** and **I-Mepy**, mainly emit delayed fluorescence from the ^{1}(M+X)LCT state at room temperature. On the other hand, at low temperatures below 170 K, **Cl-Mepy**, **Br-Mepy** and **I-Mepy** emit phosphorescence from the ^{3}(M+X)LCT state because the ^{1}(M+X)LCT state cannot be thermally activated at the expense of the ^{3}(M+X)LCT state. Thermally activation efficiency i.e., ΔE may affect the deference of luminescence quantum yield between at 298K and 77K. For complex **Cl-Mepy,** which has lowest ΔE values (940 cm^{-1}), the luminescence quantum yield decrease from 0.99 at 298K to 0.82 at 77K because TADF is suppressed at low temperature. On the other hand, the luminescence quantum yields at 77K are same or higher than compared to that at 298K for **Br-Mepy** and **I-Mepy**. The higher luminescence quantum yields at low temperature are due to lower thermally activation efficiency (i.e. larger ΔE) at room temperature and more effective suppression of non-radiative decay process (i.e. smaller k_{nr}) at low temperature compared to that at room temperature.

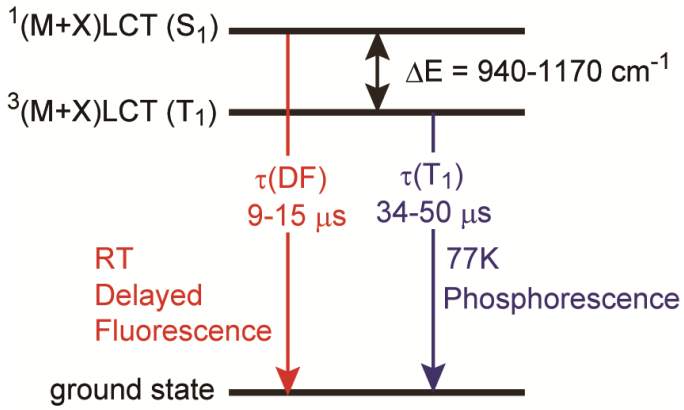

Scheme 3-2. Schematic diagram of the two-state model of **Cl-Mepy**, **Br-Mepy**, and **I-Mepy**.

3-4 Conclusion

Three mononuclear Cu(I)-halide complexes containing Mepy ligand were prepared. **Cl-Mepy**, **Br-Mepy** and **I-Mepy** show strong blue luminescence in the crystals, exhibiting almost 100% quantum yields for complexes **Cl-Mepy** and **Br-Mepy**. The emission studies and TD-DFT calculations reveal that **Cl-Mepy**, **Br-Mepy** and **I-Mepy** emit TADF from the ^{1}(M+X)LCT state at room temperature because of their small singlet–triplet energy difference. In addition, these complexes can be easily prepared from commercially available inexpensive reagents such as CuX, Mepy, and PPh_3. Such an efficient synthesis of desired strong emitters from simple starting materials without difficult procedures should be one of the important factors for their applications.

3-5 References

1 (a) L. Xiao, Z. Chen, B. Qu, J. Luo, S. Kong, Q. Gong and J. Kido, *Adv. Mater.*, 2011**, 23**, 926; (b) Y. Chi and P. -T. Chou, *Chem. Soc. Rev.*, 2010, **39**, 638.

2 (a) C. Adachi, M. A. Baldo, M. E. Thompson and S. R. Forrest, *J. Appl. Phys.*, 2001, **90**, 5048; (b) H. Sasabe, J. Takamatsu, T. Motoyama, S. Watanabe, G. Wagenblast, N. Langer, O. Molt, E. Fuchs, C. Lennartz and J. Kido, *Adv. Mater.*, 2010, **22**, 5003; (c) M. A. Baldo, D. F. O'Brien, Y. You, A. Shoustikov, S. Sibley, M. E. Thompson and S. R. Forrest, *Nature*, **1998,** *395*, 151; (d) M. A. Baldo, S. Lamansky, P. E. Burrows, M. E. Thompson and Forrest, S. R. *Appl. Phys. Lett.*, 1999**, 75**, 4; (e) Y. Kawamura, K. Goushi, J. Brooks, J. J. Brown, H. Sasabe and C. Adachi, *Appl. Phys. Lett.*, 2005, **86**, 071104.

3 (a) H. Uoyama, K. Goushi, K. Shizu, H. Nomura and C. Adachi, *Nature*, 2012, **492**, 234; (b) J. C. Deaton, S. C. Switalski, D. Y. Kondakov, R. H. Young, T. D. Pawlik, D. J. Giesen, S. B. Harkins, A. J. M. Miller, S. F. Mickenberg and J. C. Peters, *J. Am. Chem. Soc.*, 2010, **132**, 9499; (c) A. Tsuboyama, K. Kuge, M. Furugori, S. Okada, M. Hoshino and K. Ueno, *Inorg. Chem.*, 2007, **46**, 1992.

4 (a) S. Igawa, M. Hashimoto, I. Kawata, M. Yashima, M. Hoshino and M. Osawa, *J. Mater. Chem. C*, 2013, **1**, 542; (b) Q. Zhang, T. Komino, S. Huang, S. Matsunami, K. Goushi and C. Adachi, *Adv. Funct. Mater.*, 2012, **22**, 2327.

5 (a) Q. Zhang, J. Li, K. Shizu, S. Huang, S. Hirata, H. Miyazaki and C. Adachi, *J. Am. Chem. Soc.*, 2012, **134**, 14706; (b) R. Czerwieniec, J. Yu and H. Yersin, *Inorg. Chem.*, 2011, **50**, 8293; (c) M. J. Leitl, F. R. Kuchle, H. A. Mayer, L. Wesemann and H. Yersin, *J. Phys. Chem. A*, 2013, **117**, 11823; (d) X. -L. Chen, R. Yu, Q. -K. Zhang, L. -J. Zhou, X. -Y. Wu, Q. Zhang and C. -Z. Lu, *Chem. Mater.*, 2013, **25**, 3910.

6 R. Czerwieniec, K. Kowalski and H. Yersin, *Dalton Trans.*, 2013, **42**, 9826.

7 (a) H. Araki, K. Tsuge, Y. Sasaki, S. Ishizaka and N. Kitamura, *Inorg. Chem.*, 2005, **44**, 9667; (b) D. M. Zink, D. Volz, T. Baumann, M. Mydlak, H. Flügge, J. Friedrichs, M.

Nieger and S. Bräse, *Chem. Mater.*, 2013, **25**, 4471; (c) D. M. Zink, M. Bächle, T. Baumann, M. Nieger, M. Kuhn, C. Wang, W. Klopper, U. Monkowius, T. Hofbeck, H. Yersin and S. Bräse, *Inorg. Chem.*, 2013, **52**, 2292.

8 T. Kräuter and B. Neumüller, *Polyhedron*, 1996, **15**, 2851.

9 (a) W. R. Dawson and M. W. Windsor, *J. Phys. Chem.*, 1968, **72**, 325; W. H. Melhuish, *J. Phys. Chem.*, 1961, **65**, 229.

10 *CrystalClear*, Molecular Structure Corporation, Orem, UT, 2001.

11 *SIR-2004*: M. C. Burla, R. Caliandro, M. Camalli, B. Carrozzini, G. L. Cascarano, L. De Caro, C. Giacovazzo, G. Polidori and R. Spagna, *J. Appl. Crystallogr.*, 2005, **38**, 381.

12 *SIR-97*: A. Altomare, M. C. Burla, M. Camalli, G. L. Cascarano, C. Giacovazzo, A. Guagliardi, A. G. Moliterni, G. Polidori and R. Spagna, *J. Appl. Crystallogr.*, 1999, **32**, 115.

13 *SIR-2002*: M. C. Burla, M. Camalli, B. Carrozzini, G. L. Cascarano, C. Giacovazzo, G. Polidori and R. Spagna, *J. Appl. Crystallogr.*, 2003, **36**, 1103.

14 *SHELX97*: G. M. Sheldrick, *Acta Crystallogr., Sect. A:Fundam. Crystallogr.,* 2008, **64**, 112.

15 *CrystalStructure 4.0*: Rigaku Corporation, Tokyo, Japan, 2000-2010.

16 (a) A. D. Becke, *J. Chem. Phys.*, 1993, **98**, 5648; (b) C. Lee, W. Yang and R. G. Parr, *Phys. Rev.B*, 1988, **37**, 785.

17 (a) P. J. Hay and W. R. Wadt, *J. Chem. Phys.*, 1985, **82**, 270; (b) W. R. Wadt and P. J. Hay, *J. Chem. Phys.*, 1985, **82**, 284; (c) P. J. Hay and W. R. Wadt, *J. Chem. Phys.*, 1985, **82**, 299.

18 M. J. Frisch, G. W. Trucks, H. B. Schlegel, G. E. Scuseria, M. A. Robb, J. R. Cheeseman, J. A. Montgomery, Jr., T. Vreven, K. N. Kudin, J. C. Burant, J. M. Millam, S. S. Iyengar, J. Tomasi, V. Barone, B. Mennucci, M. Cossi, G. Scalmani, N. Rega, G. A. Petersson, H. Nakatsuji, M. Hada, M. Ehara, K. Toyota, R. Fukuda, J. Hasegawa, M. Ishida, T. Nakajima, Y. Honda, O. Kitao, H. Nakai, M. Klene, X. Li, J. E. Knox, H. P. Hratchian, J. B. Cross, C. Adamo, J. Jaramillo, R. Gomperts, R. E. Stratmann, O. Yazyev, A. J. Austin, R. Cammi, C. Pomelli, J. W. Ochterski, P. Y. Ayala, K. Morokuma, G. A. Voth, P. Salvador, J. J. Dannenberg, V. G. Zakrzewski, S. Dapprich, A. D. Daniels, M. C. Strain, O. Farkas, D. K. Malick, A. D. Rabuck, K. Raghavachari, J. B. Foresman, J. V. Ortiz, Q. Cui, A. G. Baboul, S. Clifford, J. Cioslowski, B. B. Stefanov, G. Liu, A. Liashenko, P. Piskorz, I. Komaromi, R. L. Martin, D. J. Fox, T. Keith, M. A. Al-Laham, C. Y. Peng, A. Nanayakkara, M. Challacombe, P. M. W. Gill, B. Johnson, W. Chen, M. W. Wong, C. Gonzalez and J. A. Pople, *Gaussian 03 (Revision E.01)*, Gaussian, Inc., Wallingford CT, 2004.

19 M. D. Hanwell, D. E. Curtis, D. C. Lonie, T. Vandermeersch, E. Zurek and G. R. Hutchison, *J. Cheminform.,* 2012, **4**, 17.

20 J. R. Lakowicz, *Principles of Fluorescence Spectroscopy*, Springer, New York, 2006, pp. 141-142.

21 J. R. Kirchhoff, R. E. Gamache Jr, M. W. Blaskie, A. A. Del Paggio, R. K. Lengel and D. R. McMillin, *Inorg. Chem.*, 1983, **22**, 2380.

22 M. S. Asano, K. Tomiduka, K. Sekizawa, K. Yamashita and K. Sugiura, *Chem. Lett.*, 2010, **39**, 376.

Chapter 4

Effects of N-heteroaromatic ligands on the photoluminescence properties of mononulclear copper(I)-halide complexes

4-1 Introduction

In chapters 2 and 3, simple manual grinding synthesis and strong blue emitters based on thermally activated delayed fluorescence (TADF) of mononuclear Cu(I)-halide complexes $[CuX(PPh_3)_2(L)]$ were discussed. These complexes are prepared by only grinding raw materials (CuX, PPh_3, L) without organic solvent and exhibit high luminescence quantum yields of ~0.99, thus mononuclear Cu(I)-halide complexes are potentially applied for easily prepared luminescent devices. For the application of these devices, it is important to control the emission properties such as emission color, lifetimes and quantum yields. In chapter 3, it became obvious that $[CuX(PPh_3)_2(Mepy)]$ ($X = Cl^-$, Br^-, I^-; Mepy = 4-methylpyridine) exhibit delayed fluorescence from singlet metal-to-ligand (Mepy) charge transfer (^{1}MLCT) combined with halide-to-ligand (Mepy) charge transfer (^{1}XLCT) state (^{1}(M+X)LCT) at room temperature, thus N-heteroaromatic ligands are expected to exert influence on the emission properties of $[CuX(PPh_3)(L)]$. In this chapter, with the aim of understanding the effect of replacement of N-heteroaromatic ligands on the emission properties, I prepared the mononuclear Cu(I)-halide complexes, $[CuX(PPh_3)_2(L)]$ (Scheme 4-1; $X = Cl^-$, Br^-, I^-; L = 4-methylpyridine (Mepy), isoquinoline (iq), 1,6-naphthyridine (nap)) and investigated their photoluminescence properties in detail. These complexes shows strong emission with quantum yields of 0.16-0.99 and the emission color of the complexes varies from red to blue depending on N-heteroaromatic ligands and halide anion. In addition, emissive excited states of these complexes also depend on N-heteroaromatic ligands.

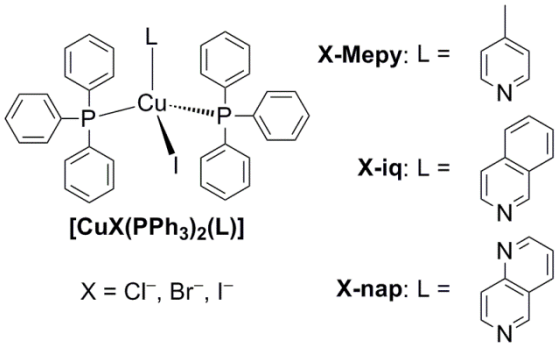

Scheme 4-1. Structure of $[CuX(PPh_3)_2(L)]$.

4-2 Experimental

4-2-1 Materials and synthesis

All commercially available starting materials were used as received and solvents were used without any purification. Unless otherwise stated, all manipulations were conducted in air. $[CuCl(PPh_3)_3]\cdot CH_3CN$,[1] $[CuBr(PPh_3)_3]$,[2] $[CuI(PPh_3)_3]$[3] are prepared according to the litureture. Synthetic procedure of $[CuX(PPh_3)_2(Mepy)]$ (**X-Mepy**, X = Cl^-, Br^-, I^-), and $[CuI(PPh_3)_2(nap)]$ (**I-nap**) were described in chapters 2 and 3. Synthetic procedure of $[CuI(PPh_3)_2(iq)]$ (**I-iq-α**) are also described in chapter 2, but polymorphic crystal of **I-iq** (**I-iq-β**) is obtained depending on the amount of PPh_3 and solvent. The preparation of **I-iq-β** was described below. The ^{1}H NMR spectrum of each sample was measured using a JEOL EX-270 NMR spectrometer at room temperature. Elemental analysis was conducted at the analysis center at Hokkaido University.

$[CuCl(PPh_3)_2(iq)]$ (Cl-iq) (iq = isoquinoline)

To $[CuCl(PPh_3)_3]\cdot CH_3CN$ (90.4 mg, 0.098 mmol) was added iq (1 mL) and then $CHCl_3$ (1 mL). Yellow crystals were obtained by slow diffusion of diethyl ether vapor into the solution overnight. Yield. 43.8 mg, 60%. Elemental analysis calculated for $C_{45}H_{37}CuClNP_2$: C, 71.80; H, 4.95; N, 1.86; found C, 71.86; H, 4.74; N, 1.91. ^{1}H NMR (270 MHz, CHLOROFORM-*d*) δ ppm 7.19 - 7.44 (m, 30 H) 7.56 - 7.78 (m, 3 H) 7.82 (d, *J*=8.2 Hz, 1 H) 7.94 (d, *J*=8.2 Hz, 1 H) 8.53 (s, 1 H) 9.27 (s, 1 H).

$[CuBr(PPh_3)_2(iq)]$ (Br-iq)

To a suspension of CuBr (37.5 mg, 0.24 mmol) in iq (1 mL) was added PPh_3 (153.8 mg, 0.59 mmol). $CHCl_3$ (2 mL) was added to the reaction mixture and then filtered to remove precipitate. Yellow crystals were obtained by slow diffusion of diethyl ether vapor into the solution overnight. Yield. 128.7 mg, 69%. Elemental analysis calculated for $C_{45}H_{37}CuBrNP_2$: C, 67.80; H, 4.68; N, 1.76; found C, 67.66; H, 4.49; N, 1.78. ^{1}H NMR (270 MHz, CHLOROFORM-*d*) δ ppm 7.15 - 7.45 (m, 30 H) 7.57 - 7.75 (m, 3 H) 7.83 (d, *J*=7.9 Hz, 1 H) 7.94 (d, *J*=7.6 Hz, 1 H) 8.52 (d, *J*=5.6 Hz, 1 H) 9.27 (s, 1 H).

$[CuI(PPh_3)_2(iq)]$ (I-iq-β)

To a suspension of CuI (48.9 mg, 0.26 mmol) in iq (1 mL) was added PPh_3 (660 mg, 2.5 mmol) and then $CHCl_3$ (1 mL). Yellow crystals were obtained by slow diffusion of diethyl ether vapor into the solution overnight. Yield. 177.1 mg, 85%. Elemental analysis calculated for $C_{45}H_{37}CuINP_2$: C, 64.02; H, 4.42; N, 1.66; found C, 64.28; H, 4.23; N, 1.68. ^{1}H NMR (270 MHz, CHLOROFORM-*d*) δ ppm 7.06 - 7.49 (m, 30 H) 7.58 - 7.76 (m, 3 H) 7.83 (d, *J*=8.2 Hz, 1 H) 7.96 (d, *J*=8.2 Hz, 1 H) 8.54 (d, *J*=5.9 Hz, 1 H) 9.27 (s, 1 H).

[CuCl(PPh$_3$)$_2$(nap)] (Cl-nap) (nap = 1,6-naphthyridine)

To [CuCl(PPh$_3$)$_3$]· CH$_3$CN (49.6 mg, 0.054 mmol) was added a CHCl$_3$ solution (1 mL) of nap (100 mg, 0.77 mmol). Yellow crystals were obtained by slow diffusion of diethyl ether vapor into the solution for 3 days. Yield. 20.5 mg, 52%. Elemental analysis calculated for $C_{44}H_{36}CuClN_2P_2$: C, 70.12; H, 4.81; N, 3.72; found C, 70.17; H, 4.67; N, 3.76. ^{1}H NMR (270 MHz, CHLOROFORM-*d*) δ ppm 7.20 - 7.43 (m, 30 H) 7.56 (dd, *J*=8.2, 4.3 Hz, 1 H) 7.93 (d, *J*=5.9 Hz, 1 H) 8.26 - 8.37 (m, 1 H) 8.75 (d, *J*=5.9 Hz, 1 H) 9.13 (dd, *J*=4.3, 2.0 Hz, 1 H) 9.32 (s, 1 H)

[CuBr(PPh$_3$)$_2$(nap)] (Br-nap)

To [CuBr(PPh$_3$)$_3$] (56.8 mg, 0.061 mmol) was added a CHCl$_3$ solution (1 mL) of nap (100 mg, 0.77 mmol). Yellow crystals were obtained by slow diffusion of diethyl ether vapor into the solution overnight. Yield. 43.1 mg, 89%. Elemental analysis calculated for $C_{44}H_{36}CuClN_2P_2$: C, 66.21; H, 4.55; N, 3.51; found C, 66.10; H, 4.47; N, 3.48. ^{1}H NMR (270 MHz, CHLOROFORM-*d*) δ ppm 7.13 - 7.46 (m, 30 H) 7.56 (dd, *J*=8.6, 4.3 Hz, 1 H) 7.92 (d, *J*=5.9 Hz, 1 H) 8.25 – 8.36 (m, 1 H) 8.75 (d, *J*=5.9 Hz, 1 H) 9.13 (dd, *J*=4.3, 2.0 Hz, 1 H) 9.32 (s, 1 H)

4-2-2 Luminescence measurements

The luminescence spectrum of each sample was measured using a JASCO FR-6600 spectrofluorometer at room temperature. The luminescence quantum yield was recorded on a Hamamatsu Photonics C9920-02 absolute photoluminescence quantum yield measurement system equipped with an integrating sphere apparatus and 150-W CW xenon light source. Hamamatsu Photonics A10095-03 non-luminescent quartz sample holder was used for absolute photoluminescence quantum yield measurement. This quantum yield measurement was performed in air atmosphere; in order to verify the reliability and accuracy of our techniques, I determined the direct quantum yield of anthracene ethanol solution using this setup and attained the correct value of 0.27.[4] Emission life time measurements were conducted by using a streak camera equipped with Hamamatsu Photonics, C4334 as a photo detector at 337 nm excitation. A liquid N_2 cryostat (Optistat-DN optical Dewar and ITC-503 temperature controller, Oxford Instruments) was used to control a sample temperature.

4-2-3 Single-crystal X-ray diffraction measurements

All single-crystal X-ray diffraction measurements were conducted using a Rigaku Mercury CCD diffractometer with graphite monochromated Mo Kα radiation (λ = 0.71069 Å) and a rotating anode generator. Each single-crystal was mounted on a MicroMount using paraffin oil. The crystal was then cooled using an N_2-flow type temperature controller. Diffraction data were collected and processed using the CrystalClear softwere.[5] Structures were solved by the direct method using SIR-2004[6] for **X-iq** (X^- = Cl^-, Br^-, I^-), **X-nap** (X^- = Cl^-, Br^-). Structural refinements were conducted by the full-matrix least-squares method using SHELXL-97.[7] Non-hydrogen atoms were refined anisotropically, and hydrogen atoms were refined using the riding model. All calculations were conducted using the Crystal Structure crystallographic software package.[8] Crystallographic data obtained for each complex are summarized in Table 4-1.

Table 4-1. Crystal parameters and refinement data.

	Cl-iq	**Br-iq**	**I-iq-β**
T / K	200 (1)	200 (1)	200 (1)
Formula	$C_{45}H_{37}ClCuNP_2$	$C_{45}H_{37}BrCuNP_2$	$C_{45}H_{37}ICuNP_2$
Formula weight	752.74	797.19	844.19
Crystal system	Triclinic	Monoclinic	Monoclinic
Space group	$P\ \overline{1}$	$P2_1/n$	$P2_1/n$
a / Å	9.694(3)	9.9964(7)	10.0363(10)
b / Å	13.320(4)	36.138(2)	35.870(4)
c / Å	15.401(4)	11.2964(8)	11.5526(10)
α / °	83.360(9)	90	90
β / °	79.997(9)	114.671(2)	114.936(3)
γ / °	77.599(9)	90	90
V / Å^3	1906.4(9)	3708.4(5)	3771.2(7)
Z	2	4	4
D_{cal} / g cm^{-3}	1.311	1.428	1.487
Reflections collected	15589	22699	21108
Unique reflections	8633	8252	8416
R_{int}	0.0542	0.0398	0.0377
GOF	1.004	1.088	1.193
R ($I > 2\sigma(I)$)	0.0514	0.0422	0.0353
Rw	0.1271	0.0915	0.0944

	Cl-nap	**Br-nap**
T / K	200 (1)	200 (1)
Formula	$C_{44}H_{36}ClCuN_2P_2$	$C_{44}H_{36}BrCuN_2P_2$
Formula weight	753.73	798.18
Crystal system	Monoclinic	Monoclinic
Space group	$P2_1/n$	$P2_1/n$
a / Å	9.8962(8)	9.906(2)
b / Å	36.755(2)	36.302(8)
c / Å	11.1003(10)	11.286(3)
α / °	90	90
β / °	114.926(4)	114.563(2)
γ / °	90	90
V / Å^3	3661.5(5)	3691(2)
Z	4	4
D_{cal} / g cm^{-3}	1.367	1.436
Reflections collected	39704	22761
Unique reflections	8323	8137
R_{int}	0.0346	0.0304
GOF	1.078	1.263
R ($I > 2\sigma(I)$)	0.0377	0.0396
Rw	0.0857	0.1049

4-2-4 Theoretical Calculations

DFT calculations were performed with B3LYP functional[9] and the LANL2DZ basis[10] set using Gaussian 03 program.[11] Molecular structures determined by X-ray crystallographic analysis were used. Molecular orbital are shown using Avogadro 1.10.[12]

4-3 Results and discussion

4-3-1 Crystal structures

Figures 4-1 and 4-2 show the molecular structures of **X-iq** and **X-nap** (X = Cl^-, Br^-), respectively. The molecular structures and crystal parameter of **I-iq-α** and **I-nap** are shown in chapter 2. Selected bond lengths and angles around copper(I) atom are listed in Table 4-2. Cu ions in all complexes commonly took tetrahedral coordination geometry occupied by one halide, one N atom of N-heteroaromatic ligand and two P atoms of PPh_3 ligand, which is the characteristic structure to the Cu(I) ion.

The crystal system of **Cl-iq** and **Br-iq** are Triclinic $P\ \bar{1}$, Monoclinic $P2_1/n$, respectively. Two kinds of **I-iq** crystals, which are named as **I-iq-α**, **I-iq-β**, are obtained depending on the synthesis condition such as amount of PPh_3 and solvent. The main difference between **I-iq-α**, **I-iq-β** are cell volume. The cell volume of **I-iq-α** and **I-iq-β** are 3864.3(16) $Å^3$ and 3771.2(7) $Å^3$, respectively. The crystal system of **I-iq-α** and **I-iq-β** are Monoclinic $P2_1/c$ and $P2_1/n$, respectively. The main difference between the molecular structure of **Cl-iq** and **X-iq** (X^- = Br^-, I^-) is conformation of iq ligand. The C37 carbon atom of **Br-iq** and **I-iq** are oriented the direction of the halide anion, while **Cl-iq** is oriented against. The reason is also probably due to the steric effect of larger halides of complexes **Br-iq** and **I-iq**. Interestingly, **Br-iq**, **I-iq-β**, **Cl-nap**, **Br-nap** and **I-nap** complexes are isomorphous to each other. The Cu-X bonds of **Cl-nap** is shorter than that of **Cl-iq** (2.3330 Å for **Cl-iq**, 2.3120 Å for **Cl-nap**) and Cu-N bonds of **Cl-nap** is longer than that of **Cl-iq** (2.091 Å for **Cl-iq**, 2.125 Å for **Cl-nap**). The shorter Cu-X bond and longer Cu-N bonds of **Cl-nap** indicate steric repulsion between Cl ion and nap ligand. Thus, the steric repulsion between halide ion and nap ligand thought to be the cause of isomorphism of **X-nap**.

Table 4-2. Selected bond distances (Å) around copper(I) ions in the complexes **X-iq** and **X-nap**.

	Cl-iq	**Br-iq**	**I-iq-*α***	**I-iq-*β***
Cu-X	2.3330(9)	2.4546(6)	2.6514(8)	2.6288(5)
Cu-N	2.091(3)	2.1223(18)	2.125(4)	2.120(2)
Cu-P1	2.2493(10)	2.2830(8)	2.2711(13)	2.2858(8)
Cu-P2	2.2671(8)	2.2781(8)	2.2782(14)	2.2807(8)

	Cl-nap	**Br-nap**	**I-nap**
Cu-X	2.3120(10)	2.4520(8)	2.6307(5)
Cu-N	2.125(3)	2.1226(19)	2.1218(17)
Cu-P1	2.2712(9)	2.2758(9)	2.2819(7)
Cu-P2	2.2709(9)	2.2741(9)	2.2821(8)

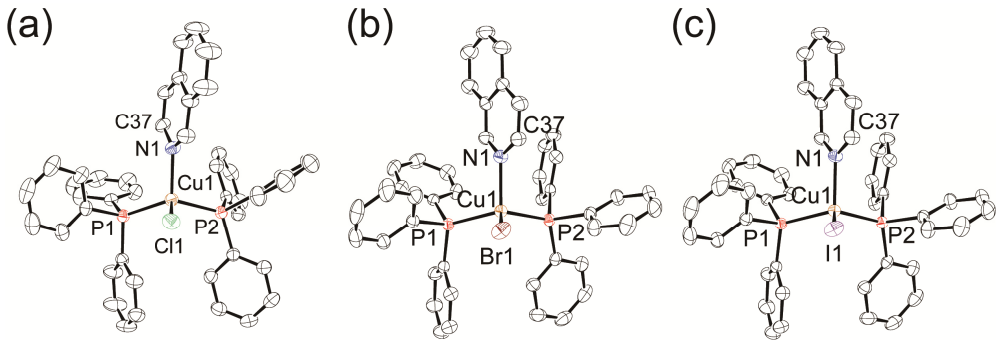

Figure 4-1. ORTEP drawings of (a) **Cl-iq**, (b) **Br-iq** and (c) **I-iq-*β***. Hydrogen atoms are omitted for clarity. Displacement parameters are drawn at 50% probability level.

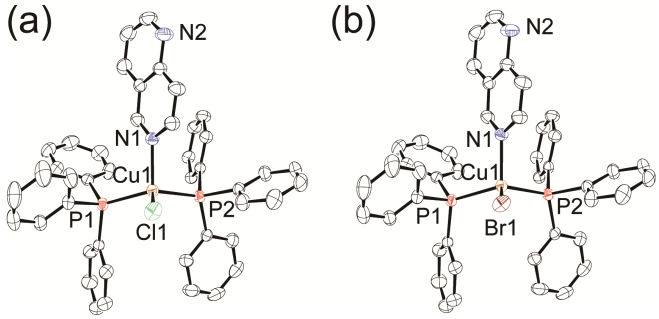

Figure 4-2. ORTEP drawings of (a) **Cl-nap** and (b) **Br-iq**. Hydrogen atoms are omitted for clarity. Displacement parameters are drawn at 50% probability level.

4-3-2 Luminescent properties

Luminescent properties of **X-Mepy** are already discussed in chapter 3; **X-Mepy** exhibit strong blue emission from ^{1}(M+X)LCT state in the crystals. To clarify the substitution effects of N-heteroaromatic and halide ligands on luminescence properties in more detail, photophysical properties of **X-iq** and **X-nap** were investigated. Figures 4-3 and 4-4 shows emission spectra of **X-iq** and **X-nap** in crystals and emission properties of **X-iq** and **X-nap** are summarized in Table 4-3. The emission properties of **X-Mepy** are shown in chapter 3. The luminescent measurement were performed with crystal samples due to the limited chemical stability in solution in analogue with other Cu(I)-halide complexes.[13]

4-3-2-1 Luminescent properties of [CuX(PPh$_3$)$_2$(iq)] complexes (X-iq)

Figure 4-3 shows the emission spectra of **X-iq** at 298 K and 77 K in the crystals. **X-iq** exhibit green to yellow emission and the emission maxima of **X-iq** at 298 K were observed at around 520 nm which is longer wavelength than that of **X-Mepy**. **Br-iq** and **I-iq-*α*** provide similar broad emission spectra without vibronic progression at 298 K, indicating that the emissive excited states have a charge-transfer character. On the other hand, the spectra of **Cl-iq** and **I-iq-*β*** have vibronic structure, suggesting that the emissive excited states have the π–π* transition character. These results indicate that the crystal structure and the halide anion affect the emissive state. At 77 K, the spectra of **X-iq** have a sharp vibronic structure irrespective of crystal structures and the halide anion. **X-iq** exhibit high luminescence quantum yields of 0.44-0.73 at 298 K. On the other hand, luminescence quantum yields of **X-iq** at 77K are 0.20-0.51, which values are lower than those at 298K. The decrease of luminescence quantum yields at low temperature are probably due to variation of the emissive state between the room temperature and low temperature; If **X-iq** emit luminescence from the same emissive state at room temperature and low temperature, the luminescence quantum yields at low temperature should be higher than those at room temperature because the non-radiative decay process are suppressed at low temperature and radiative rate constants are independent of temperature.

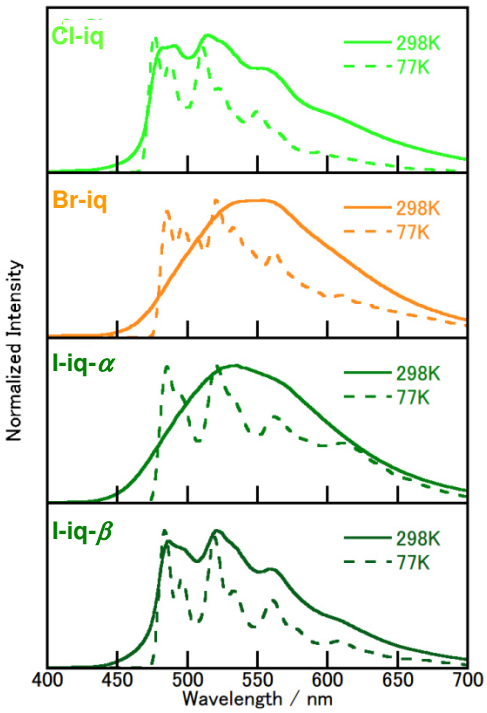

Figure 4-3. Luminescence spectra of **X-iq** in the crystals (λ_{ex} = 370 nm) at 298 K (solid line) and 77 K (dotted line).

Table 4-3. Luminescence properties of complexes **X-iq** and **X-nap** in the solid states at 298 K and 77 K.

Compound	**Cl-iq**		**Br-iq**		**I-iq-α**		**I-iq-β**	
	298 K	77 K	298 K	77 K	298 K	77 K	298 K	77 K
λ_{max} [a] (nm)	491, 515, 553	476, 488, 511, 522, 549	554	486, 497, 507, 520, 532, 561	535	486, 521, 561, 610	487, 520, 558	484, 496, 520, 532, 561, 607
τ(μs (A_n))[b]	154 (0.60)	227 (0.49)	73 (0.58)	152 (0.84)	27 (0.54)	123 (0.94)	79 (0.74)	126 (0.86)
	616 (0.48)	1436(0.54)	165 (0.47)	825 (0.23)	78 (0.52)	534 (0.18)	493 (0.30)	777 (0.23)
Φ [c]	0.77	0.56	0.46	0.20	0.63	0.51	0.65	0.50
τ_{av} [d] (μs)	506	1285	132	553	65	310	376	528
k_r [e] (s^{-1})	1.5×10^3	4.4×10^2	3.5×10^3	3.6×10^2	9.8×10^3	1.6×10^3	1.7×10^3	9.5×10^2
k_{nr} [f] (s^{-1})	4.5×10^2	3.4×10^2	4.1×10^3	1.4×10^3	5.7×10^3	1.6×10^3	9.3×10^2	9.5×10^2

Compound	**Cl-nap**		**Br-nap**		**I-nap**	
	298 K	77 K	298 K	77 K	298 K	77 K
λ_{max} [a] (nm)	636	674	608	634	571	585
τ(μs (A_n))[b]	0.32 (0.12)	3.8 (0.20)	1.6 (0.29)	21.9 (0.033)	4.7 (0.87)	46.2 (0.16)
	1.5 (0.91)	14.4 (0.84)	3.6 (1.6)	61.9 (0.97)	6.3 (0.14)	62.7 (0.84)
Φ [c]	0.16	0.08	0.44	0.25	0.73	0.63
τ_{av} [d] (μs)	1.5	14	3.5	38	5.0	73
k_r [e] (s^{-1})	1.1×10^5	5.8×10^3	1.2×10^5	6.6×10^3	1.5×10^5	8.9×10^3
k_{nr} [f] (s^{-1})	5.7×10^5	6.7×10^4	1.6×10^5	2.0×10^4	5.3×10^4	5.2×10^3

[a] Emission maximum. [b] Emission lifetime. Emission decays were analysed with two components: $I = A_1\exp(-t/\tau_1) + A_2\exp(-t/\tau_2)$. [c] Photoluminescence quantum yields in the solid states. [d] Average emission lifetimes were determined by using eq 1. [e] Radiative rate constants k_r were estimated by Φ/τ_{av}. [f] Nonradiative rate constants k_{nr} were estimated by $k_r(1 - \Phi)/\Phi$.

The emission lifetimes of complexes **X-iq** in the crystals were estimated by the least-square fitting of the emission decays using two exponentials, i.e., $I = A_1\exp(-t/\tau_1) + A_2\exp(-t/\tau_2)$, where τ_1 and τ_2 are the lifetimes, and A_1 and A_2 are the pre-exponential factors. The lifetimes of complexes **X-iq**, with the values ranging from several tens microseconds to hundreds of microseconds, are longer than that of **X-Mepy** (several to several tens microseconds) and similar to those previously reported for Cu(I) complexes such as [3,5-$(CF_3)_2$Pz]Cu(2,4,6-collidine) and [H_2B(3,5-$(CF_3)_2$Pz)$_2$]Cu(2,4,6-collidine), whose luminescence was assigned to phosphorescence from $^3\pi$–π^* aromatic ligand excited state.[14] Thus, the longer lifetimes of **X-iq** compared to **X-Mepy** suggests involvement of $^3\pi$–π^* aromatic ligand excited state.

The radiative rate constants (k_r) of complexes **X-iq** were estimated from the average emission lifetime (τ_{av}) by using equation (1) for two exponential decay components[15]:

$$\tau_{av} = \frac{A_1\tau_1^2+A_2\tau_2^2}{A_1\tau_1+A_2\tau_2} \quad (1)$$

The τ_{av} of complexes **X-iq** and k_r, which was estimated by using the relation $k_r = \Phi / \tau_{av}$, and the nonradiative rate constants k_{nr} are also listed in Table 4-3. The radiative constants of **X-iq** at 298 K (k_r = 1.5–3.5 $\times$ 10^3 s^{-1}) are 20 to 70 times smaller than that of **X-Mepy**. The different k_r value between **X-Mepy** and **X-iq** indicate that **X-iq** emit from an excited state different from that of **X-Mepy**. For **X-iq** complexes, the radiative rate constants at room temperature are several times larger than those at 77 K, indicating that the origins of the emissions at 298 and 77 K are different.

The deference of k_r value between at low temperature and room temperature confirm that the two emissive states, which are probably assigned to triplet CT state and π–π^* aromatic ligand excited state, are in thermal equilibrium.

4-3-2-2 Emission properties of [CuX(PPh_3)$_2$(nap)] complexes (X-nap)

Figure 4-4 shows the emission spectra of **X-nap** at 298 K and 77 K in the crystals. The **X-nap** exhibit yellow to red emission and emission maxima at 298 K were observed at 636, 608 and 571 nm for **Cl-nap**, **Br-nap** and **I-nap**, respectively. The emission maxima of **X-nap** are longer wavelength than that of **X-Mepy** and **X-iq**. The emission wavelengths are strongly dependent on the halide anion. The emission maxima of **X-nap** are consistent with the order of ligand field strength of the halide ion in the complexes (I^- < Br^- < Cl^-) and a similar trend was observed for more commonly used halide-bridged dinuclear complexes.[13b, 16] The spectra of **X-nap** are also broad without vibronic progressions, indicating that the emissive excited states have the charge-transfer character. Each emission spectrum at 77 K shifted to lower energies by ca. 420–890 cm^{-1} than that at room temperature.

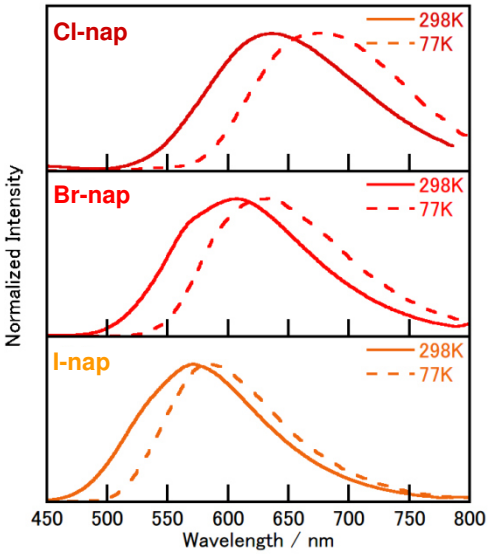

Figure 4-4. Luminescence spectra of **X-nap** in the crystals (λ_{ex} = 400 nm) at 298 K (solid line) and 77 K (dotted line).

The luminescence quantum yields of **Br-nap** and **I-nap** exhibit high luminescence quantum yields of 0.77 and 0.44, respectively. On the other hand, luminescence quantum yields of **Cl-nap** are 0.16 which value are lower than those of **Br-nap** and **I-nap**. The low emission quantum yield of **Cl-nap** is probably related to the energy gap law, i.e., a decrease in emission quantum efficiency with decreasing emission energy, since competing nonradiative processes become more relevant.[17] The luminescence quantum yields of **X-nap** at 77K are also lower (0.08 for **Cl-nap**, 0.25 for **Br-nap**, and 0.63 for **I-nap**, respectively) than those at 298K, suggesting that the emissive states at room temperature and low temperature are different.

The emission lifetimes of complexes **X-nap** in the crystals were also estimated by the least-square fitting of the emission decays using two exponentials. The lifetimes of complexes **X-nap**, with the values ranging from several to several tens microseconds, are similar to that of **X-Mepy** whose emission are assigned as the delayed fluorescence at room temperature. Therefore, the luminescence of complexes **X-nap** may have a similar origin. The radiative constants of **X-nap** at 298 K (k_r = 1.1–1.5 × 10^5 s^{-1}) are very close to those of **X-Mepy**, indicating that **X-nap** emit from an excited state similar to those of **X-Mepy**. The radiative rate constants of **X-nap** at 298 K are also ca. 20 times larger than that at 77 K. Thus, we assumed that luminescence of **X-nap** exhibit delayed fluorescence at room temperature.

To confirm the above assumption, temperature dependence of the average emission lifetimes of complexes **X-nap** was investigated. As shown in Figure 4-5, their lifetimes changed gradually at

low-temperature region below 100−120 K for **X-nap**. However, a sharp decrease in the lifetimes was observed with increase in temperature. Assuming the two-state model involving the lowest excited singlet state (S_1) and the lowest excited triplet state (T_1), the observed lifetime can be expressed as a Boltzmann average by using equation (2)[18]:

$$\tau_{obs} = \frac{3+exp(-\Delta E/RT)}{3/\tau_{T_1}+1/\tau_{S_1}exp(-\Delta E/RT)} \qquad (2)$$

where, ΔE is the energy difference between the singlet and triplet states, τ_{S1} and τ_{T1} are the lifetimes of S_1 (fluorescence) and T_1 (phosphorescence) states, R is the ideal gas constant, and T is the absolute temperature. In this two-state model analysis, average lifetime was used instead of τ_{obs}, i.e., $\tau_{obs} = \tau_{av}$. The corresponding fitting parameters are listed in Table 4-4. The obtained ΔE values 550-710 cm^{-1} for **X-nap** are roughly consistent to the spectral shifts of ~1000 cm^{-1} between 298 and 77 K, indicating that the two-state model is reasonable in the temperature region. At room temperature, the emissions of complexes **X-nap** occur mainly from the singlet state by thermal excitation. Using fitting parameters, singlet components of luminescence ($I(S_1)/I_{total}$) can estimated by using equation (3)[13b]

$$\frac{I(S_1)}{I_{total}} = 1 - \left(1 + \frac{\Phi_{S1}\tau_{T1}}{3\Phi_{T1}\tau_{S1}}exp(-\Delta E/RT)\right)^{-1} \qquad (3)$$

where, Φ_{S1} and Φ_{T1} are luminescence quantum yields of the singlet and triplet states. We approximate Φ_{S1} and Φ_{T1} by Φ at 298 K and 77 K, respectively. The estimated singlet components at 298 K are 93-94% for **X-nap**, thus **X-nap** almost emit from the singlet state at room temperature.

Table 4-4. Fitting parameters based on the two-state model (eq 2).

	Cl-nap	**Br-nap**	**I-nap**
ΔE [a]	710 cm^{-1}	670 cm^{-1}	550 cm^{-1}
$\tau(S_1)$ [b]	18 ns	51 ns	119 ns
$\tau(T_1)$ [b]	11 μs	37 μs	71 μs

[a] Energy difference between S_1 and T_1. [b] lifetimes of the S_1 and T_1 states determined by the fitting using eq 2 using the averaged emission lifetimes.

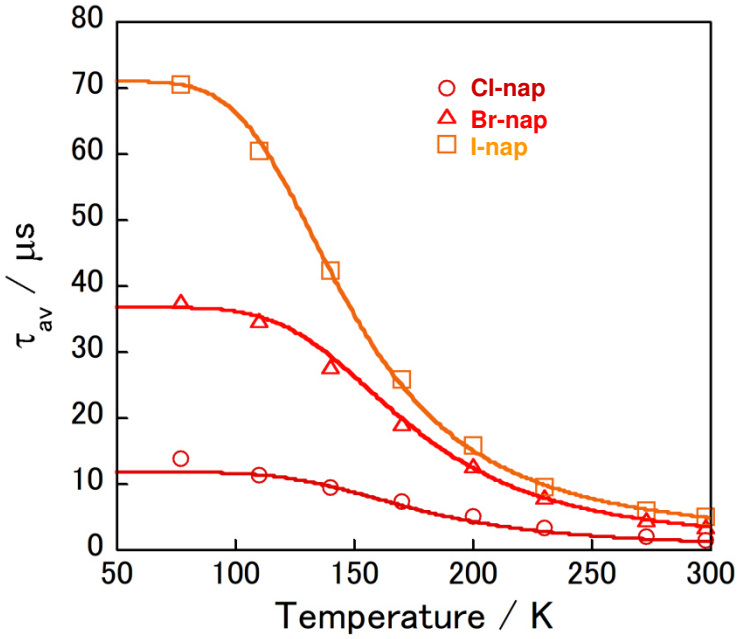

Figure 4-5. Temperature dependence of the average emission lifetimes of complexes **X-nap** in the crystals (λ_{ex} = 337 nm). The solid lines were calculated by using eq 2.

4-3-3 Theoretical Calculations

To determine the emissive excited states of complexes, time dependent-density functional theory (TD-DFT) calculations were carried out for complexes **X-iq** and **X-nap** using the atomic coordinates determined by X-ray crystallographic analysis (Figure 4-6 and 4-7). The molecular orbitals of **X-Mepy** are shown in chapter 3. The electron density in the highest occupied molecular orbital (HOMO) and HOMO-1 are distributed over the Cu and halogen atom, while that in the lowest unoccupied molecular orbital (LUMO) is localized on the L ligand. For complexes **Br-iq, I-iq, X-nap**, the HOMO-LUMO transition contributes to the lowest excited state by 100%. For complex **Cl-iq**, the HOMO-LUMO and HOMO-1 to LUMO transition are contribute to the lowest excited state by 86 and 14%, respectively. Thus, the lowest excited states of complexes **X-iq** and **X-nap** are combined MLCT and halide-to-ligand charge transfer (XLCT) states ((M+X)LCT), which are also the lowest excited states of complexes **X-Mepy**. Figure 4-8 shows schematic molecular orbital diagrams of **I-Mepy**, **I-iq** and **I-nap** and Table 4-5 are listed the calculated orbital energies of **X-Mepy**, **X-iq** and **X-nap**. As shown Figure 4-8, the HOMO energies of **I-Mepy, I-iq** and **I-nap** are almost same and independent of L ligands, while the LUMO energies of **I-Mepy, I-iq** and **I-nap** are depend on the π* energy levels of L ligands. Thus, the differences in the observed emission wavelength may be explained by the variations in the L ligand LUMOs. The other halide complexes (X = Cl^-, Br^-) also indicate a similar tendency as in Table 4-5.

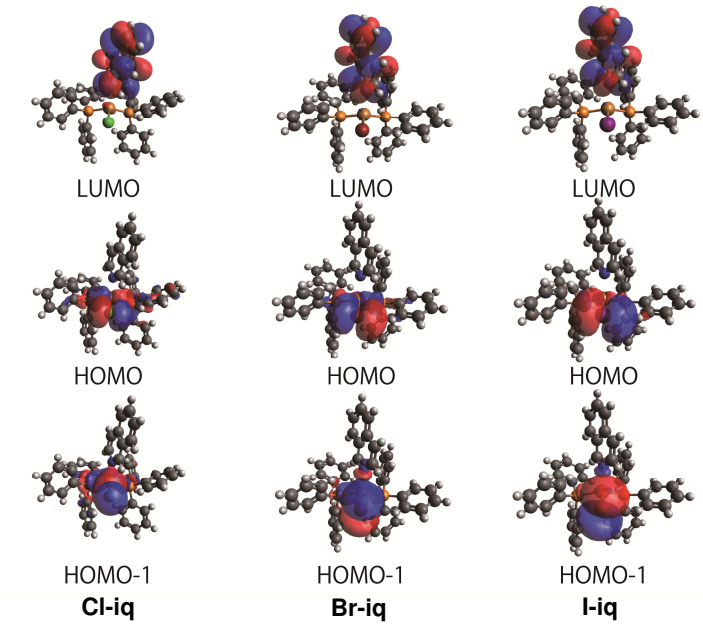

Figure 4-6. Molecular orbitals of **X-iq**.

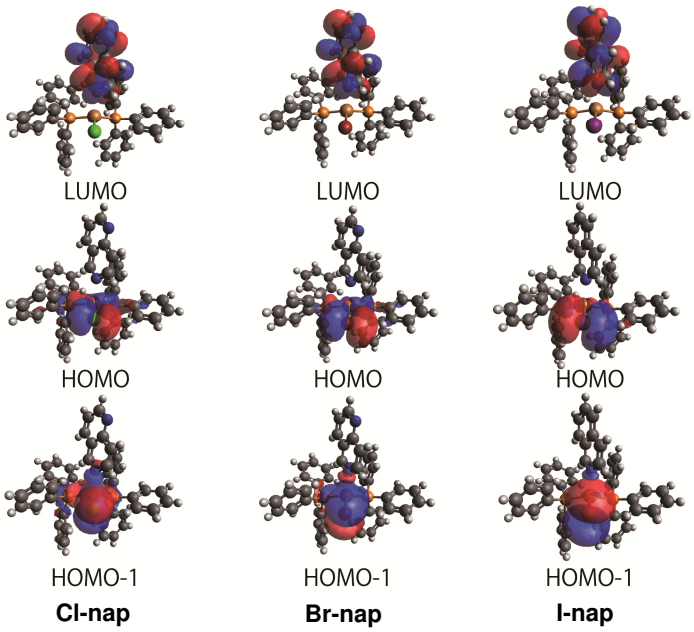

Figure 4-7. Molecular orbitals of complexes **X-nap**.

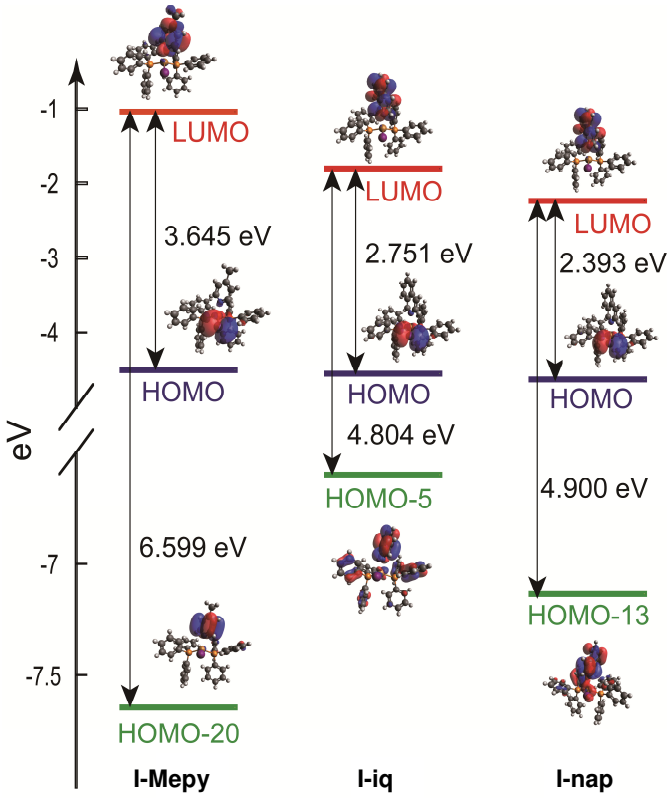

Figure 4-8. Schematic Molecular orbital diagrams of **I-Mepy, I-iq** and **I-nap**.

Although TD-DFT calculation suggest that the lowest excited state of **X-iq** are (M+X)LCT state, the emission studies indicate involvement of $^3\pi$–π^* states in emissive states of **X-iq**. To confirm why only the emissive excited states of **X-iq** have π–π* transition character, the energy difference of (M+X)LCT state and π–π* state of **I-Mepy**, **I-iq** and **I-nap** were estimated. Figure 4-8 also show the energy gap of HOMO-LUMO (**I-Mepy**, **I-iq** and **I-nap**), which are assigned to (M+X)LCT, HOMO-20 to LUMO (**I-Mepy**), HOMO-5 to LUMO (**I-iq**) and HOMO-13 to LUMO (**I-nap**), which are assigned to π–π* transition. The HOMO-LUMO energy gap (corresponded (M+X)LCT) are 3.465 eV, 2.751 eV and 2.393 eV for **I-Mepy**, **I-iq** and **I-nap**, respectively. The energy gap of HOMO-20 to LUMO (**I-Mepy**), HOMO-5 to LUMO (**I-iq**) and HOMO-13 to LUMO (**I-nap**) (corresponded π–π*) are 6.599 eV, 4.804 eV, 4.900 eV, respectively. The estimated energy difference of (M+X)LCT state and π–π* state are 3.134 eV, 2.053 eV, 2.507 eV for **I-Mepy**, **I-iq** and **I-nap**, respectively. The smallest energy difference of **I-iq** is suggests that (M+X)LCT state and π–π* state of **I-iq** are more accessible each other compared to those of **I-Mepy** and **I-iq**. Considering the experimental fact that the phosphorescence maximum of iq ligand is 520 nm[19] and emission maxima of **I-iq** are around the 520-530 nm, ^{3}(M+X)LCT and $^3\pi$–π^* state of **I-iq** are

Table 4-5. Calculated orbital energies.

Compound	HOMO-1	HOMO	LUMO
Cl-Mepy	-4.935 eV	-4.890 eV	-0.963 eV
Br-Mepy	-4.798 eV	-4.677 eV	-0.972 eV
I-Mepy	-4.624 eV	-4.508 eV	-1.043 eV
Cl-iq	-4.970 eV	-4.857 eV	-1.677 eV
Br-iq	-4.846 eV	-4.735 eV	-1.771 eV
I-iq	-4.684 eV	-4.556 eV	-1.805 eV
Cl-nap	-5.088 eV	-4.981 eV	-2.213 eV
Br-nap	-4.936 eV	-4.818 eV	-2.250 eV
I-nap	-4.764 eV	-4.627 eV	-2.234 eV

expected to be thermally accessible each other. On the other hand, those of **I-Mepy** and **I-nap** cannot be thermally accessible each other because π–π* state level of **I-Mepy** and **I-nap** are much more higher than (M+X)LCT state level of **I-Mepy** and **I-nap**.

4-3-4 Possible luminescence mechanism

Scheme 4-2 shows the schematic luminescent mechanism diagram of complexes **X-Mepy**, **X-iq** and **X-nap**. For **X-Mepy** and **X-nap**, the ^{1}(M+X)LCT state is easily thermally accessible from the ^{3}(M+X)LCT emissive state at room temperature because of the small ΔE. Thus, **X-Mepy** and **X-nap**, mainly emit delayed fluorescence from the ^{1}(M+X)LCT state at room temperature. On the other hand, at low temperatures, complexes **X-Mepy** and **X-nap** emit phosphorescence from the ^{3}(M+X)LCT state because the ^{1}(M+X)LCT state cannot be thermally activated at the expense of the ^{3}(M+X)LCT state for **X-Mepy** and **X-nap**. In contrast to **X-Mepy** and **X-nap**, the origins of the emission of **X-iq** are different. As shown in Figure 4-3, **X-iq** provides emission spectra with vibronic structure at 77 K while broad spectra with slightly or no vibronic structure depending on halide anion and crystal structure at 298 K, indicating that two emissive states are in thermal equilibrium. From the results of luminescent studies and theoretical calculations, we assumed that ^{3}(M+X)LCT and ^{3}π–π* are in thermal equilibrium and ^{3}(M+X)LCT and ^{3}π–π* component of luminescence are depend on halide anion and crystal structure at 298 K. At 77 K, repopulation of ^{3}(M+X)LCT from ^{3}π–π* is deactivated so that emission can only occur from ^{3}π–π* with a characteristic high degree of vibronic structure.

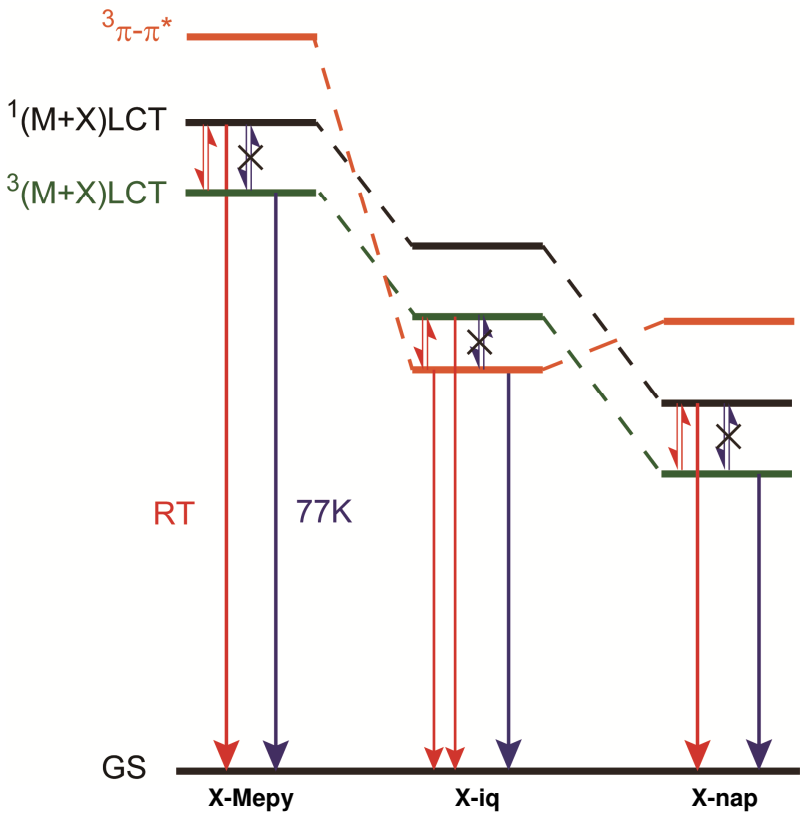

Scheme 4-2. Schematic diagram of emissive excited state of **X-Mepy**, **X-iq** and **X-nap**.

4-4 Conclusion

Luminescent properties of mononuclear copper(I)-halide complexes with N-heteroaromatic ligand, $[CuX(PPh_3)_2(L)]$ (**X-L**) (X = Cl^-, Br^-, I^-; L = Mepy, iq, nap) were investigated. All the complexes exhibit high luminescence quantum yields of 0.16-0.99 and the emission color varies from red to blue by change of L ligands and the halide anion. The emission studies and lifetime analysis revealed that the emissions of complexes **X-Mepy** and **X-nap** occur mainly from the singlet state by efficient up-conversion at room temperature. TD-DFT calculation suggest that the lowest excited states are (M+X)LCT state, thus complexes **X-Mepy** and **X-nap** emit TADF from the ^{1}(M+X)LCT state at room temperature. In contrast to **X-Mepy** and **X-nap**, the emission of **X-iq** occur from the $^3\pi$–π^* ligand excited states combined with ^{3}(M+X)LCT states at 298K and the two state component of luminescence are depend on halide anion and crystal structure. At 77K, the emission of **X-iq** occur from only the $^3\pi$–π^* ligand excited states because repopulation of ^{3}(M+X)LCT from $^3\pi$–π^* ligand excited states is suppressed.

4-5 References

1 T. Kräuter and B. Neumüller, *Polyhedron*, 1996, **15**, 2851.

2 P. O. Dunstan, *Thermochim. Acta*, 2005, **437**, 100.

3 L. Maini, D. Braga, P. P. Mazzeo and B. Ventura, *Dalton Trans.*, 2012, **41**, 531.

4 W. H. Melhuish, *J. Phys. Chem.*, 1961, **65**, 229.

5 *CrystalClear*, Molecular Structure Corporation, Orem, UT, 2001.

6 *SIR-2004*: M. C. Burla, R. Caliandro, M. Camalli, B. Carrozzini, G. L. Cascarano, L. De Caro, C. Giacovazzo, G. Polidori and R. Spagna, *J. Appl. Crystallogr.*, 2005, **38**, 381.

7 *SHELX97*: G. M. Sheldrick, *Acta Crystallogr., Sect. A:Fundam. Crystallogr.,* 2008, **64**, 112.

8 *CrystalStructure 4.0*: Rigaku Corporation, Tokyo, Japan, 2000-2010.

9 (a) A. D. Becke, *J. Chem. Phys.*, 1993, **98**, 5648; (b) C. Lee, W. Yang and R. G. Parr, *Phys. Rev. B*, 1988, **37**, 785.

10 (a) P. J. Hay and W. R. Wadt, *J. Chem. Phys.*, 1985, **82**, 299; (b) *J. Chem. Phys.*, 1985, **82**, 270; (c) W. R. Wadt and P. J. Hay, *J. Chem. Phys.*, 1985, **82**, 284.

11 M. J. Frisch, G. W. Trucks, H. B. Schlegel, G. E. Scuseria, M. A. Robb, J. R. Cheeseman, J. A. Montgomery, Jr., T. Vreven, K. N. Kudin, J. C. Burant, J. M. Millam, S. S. Iyengar, J. Tomasi, V. Barone, B. Mennucci, M. Cossi, G. Scalmani, N. Rega, G. A. Petersson, H. Nakatsuji, M. Hada, M. Ehara, K. Toyota, R. Fukuda, J. Hasegawa, M. Ishida, T. Nakajima, Y. Honda, O. Kitao, H. Nakai, M. Klene, X. Li, J. E. Knox, H. P. Hratchian, J. B. Cross, C. Adamo, J. Jaramillo, R. Gomperts, R. E. Stratmann, O. Yazyev, A. J. Austin, R. Cammi, C. Pomelli, J. W. Ochterski, P. Y. Ayala, K. Morokuma, G. A. Voth, P. Salvador, J. J. Dannenberg, V. G. Zakrzewski, S. Dapprich, A. D. Daniels, M. C. Strain, O. Farkas, D. K. Malick, A. D. Rabuck, K. Raghavachari, J. B. Foresman, J. V. Ortiz, Q. Cui, A. G. Baboul, S. Clifford, J. Cioslowski, B. B. Stefanov, G. Liu, A. Liashenko, P. Piskorz, I. Komaromi, R. L. Martin, D. J. Fox, T. Keith, M. A. Al-Laham, C. Y. Peng, A. Nanayakkara, M. Challacombe, P. M. W. Gill, B. Johnson, W. Chen, M. W. Wong, C. Gonzalez and J. A. Pople, *Gaussian 03 (Revision E.01)*, Gaussian, Inc., Wallingford CT, 2004.

12 M. D. Hanwell, D. E. Curtis, D. C. Lonie, T. Vandermeersch, E. Zurek and G. R. Hutchison, *J. Cheminform.*, 2012, **4**, 17.

13 (a) H. Araki, K. Tsuge, Y. Sasaki, S. Ishizaka and N. Kitamura, *Inorg. Chem.*, 2005, **44**, 9667; (b) M. J. Leitl, F. R. Kuchle, H. A. Mayer, L. Wesemann and H. Yersin, *J. Phys. Chem. A*, 2013, **117**, 11823.

14 M. A. Omary, M. A. Rawashdeh-Omary, H. V. Diyabalanage and H. V. Dias, *Inorg. Chem.*, 2003, **42**, 8612.

15 J. R. Lakowicz, *Principles of Fluorescence Spectroscopy*, Springer, New York, 2006.

16 (a) A. Tsuboyama, K. Kuge, M. Furugori, S. Okada, M. Hoshino and K. Ueno, *Inorg. Chem.*, 2007, **46**, 1992.; (b) D. M. Zink, M. Bachle, T. Baumann, M. Nieger, M. Kuhn, C. Wang, W. Klopper, U. Monkowius, T. Hofbeck, H. Yersin and S. Bräse, *Inorg. Chem.*, 2013, **52**, 2292

17 (a) C. T. Cunningham, K. L. H. Cunningham, J. F. Michalec and D. R. McMillin, *Inorg. Chem.*, 1999, **38**, 4388; (b) J. V. Caspar and T. J. Meyer, *J. Am. Chem. Soc.*, 1983, **105**, 5583.

18 (a) Q. Zhang, T. Komino, S. Huang, S. Matsunami, K. Goushi and C. Adachi, *Adv. Funct. Mater.*, 2012, **22**, 2327; (b) R. Czerwieniec, K. Kowalski and H. Yersin, *Dalton Trans.*, 2013, **42**, 9826; (c) J. R. Kirchhoff, R. E. Gamache, M. W. Blaskie, A. A. Del Paggio, R. K. Lengel and D. R. McMillin, *Inorg. Chem.*, 1983, **22**, 2380.

19 (a) D. W. Abbott and T. Vo-Dinh, *Anal. Chem.*, 1985, **57**, 41; (b) A. M. Alak and T. Vo Dinh, *Anal. Chem.*, 1988, **60**, 596.

Chapter 5

General conclusion

5-1 General conclusion

In this thesis, luminescent properties of mononuclear Cu(I)-halide complexes with N-heteroaromatic ligands (L) [$CuX(PPh_3)_2(L)$] (X = Cl^-, Br^-, I^-) were described.

In chapter 1, the background, the aim, and the significance of the studies were surveyed focusing on luminescent metal Cu(I) complexes, thermaly activated delayed fluorescence (TADF), and mechanochemical synthesis.

In chapter 2, the grinding synthesis of [$CuI(PPh_3)_2(L)$] (L = isoquinoline (iq), 1,6-naphthyridine (nap) and pyridine (py)) were demonstrated and the luminescence properties of three mononuclear Cu(I)-iodide complexes were investigated. These complexes were synthesized by only simple grinding of CuI, PPh_3 and L using mortar and pestle for a few minutes with high yields (63-93%). The optimal synthetic condition depend on the type of L. For example, syntheses of [$CuI(PPh_3)_2(iq)$] and [$CuI(PPh_3)_2(nap)$] were synthesized by grinding CuI and PPh_3 in more than or equal to 3 eq of L, while [$CuI(PPh_3)_2(py)$] was synthesized by stepwise synthesis: First, CuI was ground with 20 eq of py for a few minutes, and then 3 eq of PPh_3 was added to the mixture and ground for additional several minutes. The different reactivity in the grinding synthesis might be related with the difference in the viscosity of L. These three complexes exhibit different colors of luminescence depending on L performing very high quantum yields (0.63–0.99).

In chapter 3, simple and extremely efficient blue emitters based on mononuclear Cu(I)-halide complexes with delayed fluorescence, [$CuX(PPh_3)_2(Mepy)$] (X = Cl^-, Br^-, I^-, Mepy = 4-methylpyridine) were discussed. They exhibit blue light emission with extremely high photoluminescence quantum yields, approaching 100% in the crystals. The emission lifetime analyses and density functional theory calculations reveal that the bright blue light emission at room temperature originates from delayed fluorescence caused by the singlet metal-to-ligand charge transfer (MLCT) state combined with the halide-to-ligand charge transfer (XLCT) state, (^{1}(M+X)LCT), which is generated by thermal activation from the ^{3}(M+X)LCT transition state because of small singlet–triplet energy differences (ΔE = 940–1170 cm^{-1}).

In chapter 4, to understand the effect of replacement of N-heteroaromatic ligands on the emission properties, photoluminescence properties of [$CuX(PPh_3)_2(L)$] (X = Cl^-, Br^-, I^-; L = Mepy, iq, nap) were described. The emission color of [$CuX(PPh_3)_2(L)$] varies from red to blue by change of L ligands and the halide anion and exhibit high emission quantum yields of 0.16-0.99 in the crystals. The emission studies and time dependent-density functional theory (TD-DFT) calculations reveal that the emission of [$CuX(PPh_3)_2(Mepy)$] and [$CuX(PPh_3)_2(nap)$] at room temperature originates from delayed fluorescence caused by the singlet metal-to-ligand charge transfer (MLCT) state combined with the halide-to-ligand charge transfer (XLCT) state, (^{1}(M+X)LCT), which is generated by thermal activation from the ^{3}(M+X)LCT transition state because of small singlet–triplet energy differences (ΔE = 550–1170 cm^{-1}). On the other hand, the emission of [$CuX(PPh_3)_2(iq)$] occurs from

the $^3\pi$–π^* ligand excited states combined with ^{3}(M+X)LCT states at room temperature. At 77 K, the emission of [CuX(PPh_3)$_2$(iq)] occur from only the $^3\pi$–π^* ligand excited states because repopulation of ^{3}(M+X)LCT from $^3\pi$–π^* ligand excited states is suppressed.

Finally, I have shown in this thesis that mononuclear Cu(I)-halide complexes are good candidate for alternative luminescent noble-metal complexes because of easy preparation and strong emission. Although applications of luminescent Cu(I) complexes are still difficult because of their instability in solution, the studies of luminescence mononuclear Cu(I)-halide complexes provide simple synthetic approach of luminescent materials and some knowledge about design of luminescent Cu(I) complexes.

Acknowledgement

This study on this thesis has been carried out under the direction of Professor Masako Kato during October 2011-September 2014 at the Graduate School of Chemical Sciences and Engineering, Hokkaido University.

I owe my deepest gratitude to Professor Masako Kato for her earnest guidance and proper suggestions. I would like to express my gratitude to Professor Ho-Chol Chang (present address, Chuo University), and Dr. Atsushi Kobayashi and Dr. Masaki Yoshida for invaluable suggestion and discussions. I am deeply grateful to Professor Noboru Kitamura, Professor Tetsuya Taketsugu and Professor Yasuchika Hasegawa for reviewing this thesis.

I am thankful to Ms. Mayu Shimizu and Ms. Mariko Tsukada for their secretarial works. I would like to thank Dr. Takeshi Matsumoto for helpful advice. I am indebted to Dr. Tadashi Ohba and Dr. Rie Sakurai for fruitful discussion and kind comments. Special thanks also to all members of the group of Professor Masako Kato for their friendship during the time in the laboratory.

I am much indebted for the financial support of Global COE program for doctoral students.

Finally, I would like to express special thanks to my parents for their supports and encouragement.

Hiroki Ohara
Graduate School of Chemical Sciences and Engineering, Hokkaido University